UvA-DARE (Digital Academic Repository)

Indirect searches for decaying dark matter

Ibarra, A.; Tran, D.; Weniger, C.

Link to publication

arXiv:1307.6434v2 [hep-ph] 7 Nov 2013

INDIRECT SEARCHES FOR DECAYING DARK MATTER

ALEJANDRO IBARRA

Physik-Department, Technische Universität München, James-Franck-Straße 1
85748 Garching, Germany
ibarra@tum.de

DAVID TRAN

School of Physics and Astronomy, University of Minnesota, Tate Lab, 116 Church Street SE
Minneapolis, MN 55455, U.S.A.
tran@physics.umn.edu

CHRISTOPH WENIGER

GRAPPA Institute, University of Amsterdam, Science Park 904
1098XH Amsterdam, Netherlands
c.weniger@uva.nl

Numerous observations point towards the existence of an unknown elementary particle with no electromagnetic interactions, a large population of which was presumably produced in the early stages of the history of the Universe. This so-called dark matter has survived until the present day, accounting for the 26% of the present energy budget of the Universe. It remains an open question whether the particles comprising the dark matter are absolutely stable or whether they have a finite but very long lifetime, which is a possibility since there is no known general principle guaranteeing perfect stability. In this article we review the observational limits on the lifetime of dark matter particles with mass in the GeV − TeV range using observations of the cosmic fluxes of antimatter, gamma-rays and neutrinos. We also examine some theoretically motivated scenarios that provide decaying dark matter candidates.

1. Introduction

Despite many independent pieces of evidence for the existence of dark matter particles in the Universe,[1–3] very little is known about their properties from the point of view of particle physics: The spin and the parity of the dark matter are completely unknown, while the mass, the interaction cross-section with nuclei and the dark matter lifetime are only very weakly constrained. Indeed, the cosmological and astrophysical evidence for dark matter does not require the dark matter to be absolutely stable but only to be very long-lived, with a lifetime much longer than the

Table 1.   Longest lived particles in the Standard Model of Particle Physics

Particle	Lifetime	Decay channel	Theoretical interpretation
proton	$\tau > 8.2 \times 10^{33}$ years	$p \to e^+ \pi^0$	Baryon number conservation
electron	$\tau > 4.6 \times 10^{26}$ years	$e \to \gamma\nu$	Electric charge conservation
neutrino	$\tau \gtrsim 10^{12}$ years	$\nu \to \gamma\gamma$	Lorentz symmetry conservation
neutron	$\tau = 880.0 \pm 0.9$ s	$n \to p\bar{\nu}_e e^-$	Mild breaking of isospin symmetry
dark matter	$\tau \gtrsim 10^{10}$ years	?	?

age of the Universe of about 13.8 Gyr. The search for the decay products of dark matter can be used to impose upper bounds on the decay width of dark matter into different final states. Provided that these final states dominate the decay, this implies lower bounds on the total dark matter lifetime.

None of the massive particles in the Standard Model are guaranteed to be absolutely stable on kinematical grounds alone since they could all decay into lighter matter particles and eventually into photons. Nevertheless, we clearly observe the existence of long-lived particles, the longevity of which we attribute to the conservation of certain quantum numbers.

Our first example is the *proton*, which could decay, e.g., into a positron and a neutral pion, $p \to e^+ \pi^0$. Such a decay has never been observed, despite the great efforts that have been made, resulting in an impressive lower limit on the proton lifetime of $\tau > 8.2 \times 10^{33}$ years.[4] We attribute the non-observation of this decay to the conservation of baryon number, which is an accidental symmetry of the renormalizable part of the Standard Model Lagrangian, and which could in principle be broken by higher dimensional operators. In fact, some well-motivated extensions of the Standard Model, such as Grand Unified theories or the most general Minimal Supersymmetric Standard Model (without R-parity conservation) predict the decay of the proton, thus encouraging further improvements of proton stability bounds. The second example is the *electron*, which could, e.g., decay into a neutrino and a photon, $e \to \nu\gamma$. This decay mode has been searched for by the Borexino collaboration, resulting in the lower limit on the electron lifetime of $\tau > 4.6 \times 10^{26}$ years.[5] The search for this decay serves as a test of electric charge conservation, which on theoretical grounds can be related to the invariance of the action under phase transformations of the different complex fields. The third example is the *neutrino*, which could decay into two photons, $\nu \to \gamma\gamma$. The photons produced in this decay have been searched for in the cosmic microwave background, resulting in the lower limit $\tau \gtrsim 10^{12}$ years.[6] This decay mode is a test of the conservation of angular momentum, which in turn is related to the invariance of the action under Lorentz transformations. Our last example is the *neutron*, which could decay into a proton, an electron and an electron antineutrino, $n \to p\bar{\nu}_e e^-$ (while preserving baryon number, electric charge and Lorentz symmetry). In contrast to the first three examples, neutron decay has been observed, with a lifetime of $\tau = 880.0 \pm 0.9$ s.[7] This lifetime is extraordinarily short compared to the limits on the

proton lifetime although extraordinarily long compared to other strongly interacting particles, a fact which is attributed to the mild breaking of the isospin symmetry.

While we have a good understanding of why the above four particles are very long-lived, and in the case of the electron and the neutrino possibly absolutely stable, there is no general principle that ensures the absolute stability of the dark matter particle (see Tab. 1 for a summary). In most models, dark matter stability is imposed *ad hoc* by imposing extra symmetries. But many well-motivated particle physics models exist which contain unstable, although very long-lived, dark matter particles. Following the same rationale as for the proton, it is conceivable that the dark matter stability could be due to an accidental symmetry of the renormalizable part of the Lagrangian which is broken by higher dimensional operators, which could thus induce the dark matter decay. Concretely, for a spin-1/2 dark matter particle, a 3-body decay into Standard Model fermions could be induced by a dimension six operator suppressed by a large mass scale M. Then, for $\mathcal{O}(1)$ couplings, the lifetime can be estimated to be[8]

$$\tau_{\mathrm{DM}} \sim 10^{26}\,\mathrm{s}\left(\frac{\mathrm{TeV}}{m_{\mathrm{DM}}}\right)^5\left(\frac{M}{10^{15}\,\mathrm{GeV}}\right)^4 . \tag{1}$$

Therefore, the search for the decay products of the dark matter particle potentially opens a window to physics at very high energies, as large as the Grand Unification Scale.

Assuming that the dark matter indeed has a finite lifetime τ_{DM}, the decay of dark matter particles with mass m_{DM} produces primary particles at the point of decay $\vec{r}$, with a rate per unit kinetic energy T and unit volume given by

$$Q(T,\vec{r}) = \frac{\rho_{\mathrm{DM}}(\vec{r})}{m_{\mathrm{DM}}}\sum_f \Gamma_f \frac{dN^f}{dT} , \tag{2}$$

where the sum is over the partial decay rates Γ_f, dN^f/dT is the energy spectrum of the particles produced in the decay channel f, and $\rho_{\mathrm{DM}}(\vec{r})$ is the dark matter density at the position $\vec{r}$.

At cosmological scales, and for our present purposes, we can consider the Universe as being filled with a homogeneous and isotropic non-relativistic gas of dark matter particles with a density given by

$$\rho_{\mathrm{DM}}(\vec{r}) = \Omega_{\mathrm{DM}}\rho_c , \tag{3}$$

where $\Omega_{\mathrm{DM}} = 0.26$ and $\rho_c = 4.9 \times 10^{-6}\,\mathrm{GeV\,cm^{-3}}$ is the critical density of the Universe (we adopt values determined by the Planck collaboration[9]). The distribution of dark matter particles in the Milky Way is inferred from numerical N-body simulations and is not precisely known. Some popular choices for the dark matter density profile, which illustrate the range of uncertainty in the predictions of the indirect dark matter signatures, are the Navarro-Frenk-White (NFW) profile:[10,11]

$$\rho_{\mathrm{DM}}(r) = \frac{\rho_0}{(r/r_{\mathrm{s}})[1 + (r/r_{\mathrm{s}})]^2} , \tag{4}$$

with scale radius $r_s = 24$ kpc,[12] the Einasto profile:[13–15]

$$\rho_{\mathrm{DM}}(r) = \rho_0 \exp\left[-\frac{2}{\alpha}\left(\frac{r}{r_s}\right)^\alpha\right]\,, \tag{5}$$

with $\alpha = 0.17$ and $r_s = 28$ kpc, and the much shallower isothermal profile:[16]

$$\rho_{\mathrm{DM}}(r) = \frac{\rho_0}{1 + r^2/r_s^2}\,, \tag{6}$$

with $r_s = 4.4$ kpc. In all the cases, the overall normalization factor ρ_0 is chosen to reproduce the local dark matter density $\rho_\odot = 0.39$ GeV/cm^3[17–21] with the distance $r_\odot = 8.5$ kpc of the Sun to the Galactic center.

The decay of dark matter injects energy in form of (anti-)matter, photons and neutrinos into the intergalactic and interstellar medium, with potential effects on a large number of cosmological and astrophysical observables. In general, these indirect signals exhibit less directional dependence and less amplification from regions of high dark matter density or at high redshifts than those associated with self-annihilation processes, since the production rate is linear in the dark matter density (as opposed to quadratic in the case of dark matter self-annihilation). This leads to subtle differences in search strategies and in exclusion limits which, in fact, are often weaker for decaying dark matter.

In this review we will focus on indirect searches for dark matter signals in cosmic-ray antimatter, gamma-rays and neutrinos. These observations typically provide the strongest constraints on the decay of dark matter particles with masses in the GeV–TeV range. This energy range is interesting for at least two reasons: (1) many of the theoretically well motivated scenarios for decaying dark matter are related to the electroweak scale and predict dark matter particles in this mass range, and (2) phenomenologically there is a strong overlap with indirect searches for WIMPs (weakly interacting massive particles), and it is important to understand to what extent a WIMP signal could be clearly discriminated from decaying dark matter. This review is meant to provide an overview of the relevant experimental constraints and particle physics models, and we will summarize in a self-contained way how indirect dark matter signatures can be calculated. We do not discuss sterile neutrino dark matter with keV-scale masses here, which constitutes a somwhat different scenario of decaying dark matter. A review of this scenario can be found in Ref. 22, 23. Indirect searches for WIMPs are discussed, e.g., in Refs. 24, 25.

This review is organized as follows: We start with a discussion of antimatter signatures, including positrons, antiprotons and antideuterons, in Section 2. Galactic and cosmological gamma-ray signals will be discussed in Section 3, followed by a brief overview of neutrino searches in Section 4. In Section 5, we discuss a selection of some interesting theoretical scenarios for decaying dark matter. We finally conclude in Section 6.

2. Antimatter Searches

Antimatter particles in the cosmic radiation are an interesting target for dark matter searches due to the relative rarity of antimatter and the fact that in typical theoretical scenarios, matter and antimatter are produced in equal amounts by dark matter decay (as opposed to ordinary astrophysical processes, which produce little to no antimatter). Processes involving the creation of primary cosmic rays from dark matter decay may thus alter the observed abundances of antimatter particles in the cosmic radiation in an appreciable way, thus allowing for indirect detection of dark matter.

Cosmic rays can be divided into two categories: primary cosmic rays originating in astrophysical sources, presumably supernova remnants, which accelerate the cosmic-ray particles to high energies; and secondary cosmic rays, which are produced by spallation processes of primary cosmic rays on the interstellar medium. Dark matter decay may constitute another primary source of primary cosmic rays. If the rate of dark matter-induced cosmic-ray production is high enough, these fluxes could be observable in the form of a deviation from the expected astrophysical background. Even in the case that a dark matter contribution to the cosmic radiation cannot be clearly identified, the measured fluxes can be used to impose constraints on particle physics models of dark matter.

In order to predict the locally observable effects of antimatter production from dark matter decay, one needs to accurately model the propagation of these particles from their point of production to our position in the Galaxy. Antimatter particles, after being created by dark matter decay, propagate in a complicated manner through the Galaxy before reaching the Earth. The most important effect in the propagation of charged cosmic rays is diffusion. Charged particles scatter on inhomogeneities of the tangled interstellar magnetic fields, inducing a random walk-like motion which can be modeled as a diffusion process. In addition to this, energy losses, drift, annihilation on gas particles and reacceleration processes can be relevant, depending on the particular cosmic-ray species.

Antimatter propagation in the Milky Way is commonly described via a stationary two-zone diffusion model with cylindrical boundary conditions. In this model, the number density of antiparticles as a function of momentum, position and time, $f(p, \vec{r}, t)$, satisfies the following transport equation:[26, 27]

$$\frac{\partial}{\partial t} f(p, \vec{r}, t) = Q(p, \vec{r}, t) + \vec{\nabla} \cdot (K \vec{\nabla} f - \vec{V}_c f) + \frac{\partial}{\partial p} p^2 D_{pp} \frac{\partial}{\partial p} \frac{1}{p^2} f$$

$$- \frac{\partial}{\partial p} \left[\frac{dp}{dt} f - \frac{p}{3} (\vec{\nabla} \cdot \vec{V}_c) f \right] - \frac{1}{\tau_f} f - \frac{1}{\tau_r} f . \qquad (7)$$

The terms of the right-hand side correspond to the injection of primary cosmic rays, the diffusion of cosmic rays due to scattering on magnetic inhomogeneities, convection by the Galactic wind of particles emitted by the disk, diffusive reacceleration in momentum space, continuous energy losses, adiabatic energy loss/gain,

and finally losses from fragmentation or radioactive decay of cosmic rays.

For the propagation of antimatter particles from dark matter decay, the above propagation equation can be simplified by regarding only stable primary particle species and neglecting adiabatic energy losses and reacceleration, which only play an important role at lower energies. Using these simplifications, the number density of antimatter particles as a function of kinetic energy[a] T is described by the following diffusion-loss equation, which is valid for electrons/positrons as well as antiprotons/antideuterons:

$$0 = \frac{\partial f}{\partial t} = Q(T,\vec{r}) + \vec{\nabla}\cdot[K(T,\vec{r})\vec{\nabla}f] + \frac{\partial}{\partial T}[b(T,\vec{r})f] - \vec{\nabla}\cdot[\vec{V}_c(\vec{r})f] - 2h\delta(z)\Gamma_{\text{ann}}f \ . \quad (8)$$

We assume free escape boundary conditions, i.e., we take $f(T,\vec{r},t) = 0$ at the boundary of the magnetic diffusion zone, the shape of which is commonly approximated by a cylinder with half-height in the range $L \simeq 1 - 15$ kpc and radius $R \simeq 20$ kpc.

The first term on the right hand side of the transport equation, $Q(T,\vec{r})$, is the source term for antiparticles from dark matter decay, Eq. (2), which was discussed in Section 1. The second term is a diffusion term, which accounts for the propagation of cosmic rays through the tangled Galactic magnetic fields. The diffusion coefficient $K(T,\vec{r})$ is often assumed to be constant throughout the diffusion zone and is usually parametrized in the following form:[27]

$$K(T) = K_0\,\beta\,\mathcal{R}^\delta \ , \quad (9)$$

where $\beta \equiv v/c$ with v being the velocity, and $\mathcal{R}$ is the rigidity of the particle, which is defined as the momentum in GeV per unit charge, $\mathcal{R} \equiv p(\text{GeV})/Z$. The normalization K_0 and the spectral index δ of the diffusion coefficient are related to the properties of the interstellar medium and can be determined from measurements of primary-to-secondary flux ratios of other cosmic-ray species, mainly from the Boron to Carbon (B/C) ratio.[28] The third term accounts for energy losses due to inverse Compton scattering on starlight or the cosmic microwave background, as well as synchrotron radiation and ionization. The fourth term is a convection term which accounts for the drift of charged particles away from the disk, which is induced by the Milky Way's Galactic wind. This wind has axial direction and is frequently assumed to be spatially constant inside the diffusion region: $\vec{V}_c(\vec{r}) = V_c\,\text{sign}(z)\,\vec{e}_z$. The fifth term accounts for antimatter annihilation with rate Γ_{ann}, when it interacts with ordinary matter in the Galactic disk, which is assumed to be an "infinitely thin" disk with half-height $h = 100$ pc.

The transport equation, using the parametrizations of the different terms given above, has a number of free parameters which have to be determined from observation. These parameters can be inferred from measurements of flux ratios of primary and secondary cosmic-ray species, with the Boron-to-Carbon ratio being the most important. Because of degeneracies in the impact of the different parameters on

---

[a]In the case of cosmic-ray nuclei, T conventionally refers to the kinetic energy per nucleon.

Table 2. Astrophysical parameters compatible with the B/C ratio that yield the minimal (MIN), median (MED) and maximal (MAX) antiproton fluxes from dark matter annihilations; taken from Ref. 28.

Model	δ	K_0 (kpc^2/Myr)	L (kpc)	V_c (km/s)
MIN	0.85	0.0016	1	13.5
MED	0.70	0.0112	4	12
MAX	0.46	0.0765	15	5

the resulting cosmic-ray fluxes, such observations cannot determine all parameters independently, resulting in uncertainties in the prediction of local fluxes, especially when those fluxes originate from outside the Galactic disk – as in the case for antimatter from decaying dark matter, which is created throughout the dark matter halo. The ranges of the astrophysical parameters that are consistent with the B/C ratio and that produce the minimal (MIN), median (MED) and maximal (MAX) antimatter fluxes were calculated in Ref. 28 and are listed in Table 2. Note, however, that recent multiwavelength studies of the latitude profile of synchrotron emission from cosmic-ray electrons disfavor diffusion zones as thin as $L \sim 1\,\mathrm{kpc}$.[29,30]

There are different approaches to solving the diffusion-loss equation, Eq. (8). In full generality the transport equation can only be solved numerically as, for example, in the well-known GALPROP[31] and DRAGON[32] codes, which employ a Crank-Nicolson implicit second-order finite-difference scheme. Alternatively, the transport equation can be solved semi-analytically by making certain simplifications and expanding the solution in a series of trigonometric and Bessel functions and approximating the full solution by a finite number of terms in the expansion. We discuss these semi-analytical solutions in detail in Appendix A.

Formally, we can write the solution of the transport equation for a particle species i at the position of the Solar System, $r = r_\odot$, $z = 0$ as as convolution involving the injection spectrum of antimatter particles and a Green's function which describes the effects of cosmic-ray transport,

$$f_i(T) = \frac{1}{m_{\mathrm{DM}}\tau_{\mathrm{DM}}} \int_0^{T_{\max}} dT'\, G_i(T, T') \frac{dN_i(T')}{dT'}\,, \tag{10}$$

where $T_{\max}$ represents the maximum kinetic energy of the antimatter particles from the decay process. We also present explicit solutions for the Green's functions and convenient numerical approximations for the particular cases of positrons and antiprotons in the appendix.

Given the number density of antimatter particles from dark matter decay as a result of the transport equation, the flux of primary antiparticles at edge of the Solar System is given by:

$$\Phi_i^{\mathrm{DM}}(T) = \frac{v}{4\pi} f_i(T). \tag{11}$$

At energies smaller than ~ 10 GeV the antimatter fluxes at the top of the Earth's atmosphere can differ considerably from the interstellar fluxes due to solar modulation effects. One frequently used parametrization of the effect of solar modulation, which can be derived from the full diffusion and convection equations describing the solar wind, is the force-field approximation.[33,34] The fluxes at the top of the atmosphere in this approximation are related to the interstellar fluxes by the following relation:[35]

$$\Phi^{\text{TOA}}(T_{\text{TOA}}) = \left(\frac{2mT_{\text{TOA}} + T_{\text{TOA}}^2}{2mT_{\text{IS}} + T_{\text{IS}}^2} \right) \Phi^{\text{IS}}(T_{\text{IS}}),\tag{12}$$

where m is the mass of the cosmic-ray antimatter particle and $T_{\text{IS}} = T_{\text{TOA}} + \phi_F$, with T_{IS} and T_{TOA} being the kinetic energies of the antimatter particles at the heliospheric boundary and at the top of the Earth's atmosphere, respectively, and ϕ_F being the Fisk potential, which varies between 500 MV and 1.3 GV over the eleven-year solar cycle.

The transport equation simplifies for the particular cases of positrons and antiprotons since some of the effects can be neglected to good approximation. We discuss these particular cases in the following.

2.1. *Positrons*

For the case of the positrons, diffusive reacceleration, convection and annihilations in the Galactic disk can be neglected in the transport equation in the energy range of interest (above ~ 10 GeV).[36,37] The transport equation then simplifies to

$$\vec{\nabla} \cdot [K(E,\vec{r})\vec{\nabla} f_{e^+}] + \frac{\partial}{\partial E}[b(E,\vec{r})f_{e^+}] + Q(E,\vec{r}) = 0 \, ,\tag{13}$$

where we identify the total energy of positrons with the kinetic energy due to the relative smallness of the electron mass.

The energy loss rate, $b(E,\vec{r})$, is dominated by inverse Compton scattering (ICS) of the positrons on the interstellar radiation field (ISRF) and by synchrotron losses on the Galactic B-field: $b = b_{\text{ICS}} + b_{\text{syn}}$. The part of the energy loss that is due to ICS is given by

$$b_{\text{ICS}}(E_e, \vec{r}) = \int_0^\infty d\epsilon \int_\epsilon^{E_\gamma^{\max}} dE_\gamma \, (E_\gamma - \epsilon) \frac{d\sigma^{\text{IC}}(E_e, \epsilon)}{dE_\gamma} f_{\text{ISRF}}(\epsilon, \vec{r}) \, ,\tag{14}$$

where $f_{\text{ISRF}}(\epsilon, \vec{r})$ is the number density of photons of the interstellar radiation field, which includes the cosmic microwave background, thermal dust radiation and starlight. An explicit model of the interstellar radiation field can be found, e.g., in Ref. 38. For an electron energy of $E_e = 1\,\text{GeV}$, b_{ICS} ranges between $4.1 \times 10^{-17}\,\text{GeVs}^{-1}$ and $1.9 \times 10^{-15}\,\text{GeVs}^{-1}$, depending on $\vec{r}$. We see that at higher energies b_{ICS} approximately scales like $\sim E_e^2$.

The synchrotron energy loss part, on the other hand, is given by

$$b_{\text{syn}}(E_e, \vec{r}) = \frac{4}{3}\sigma_{\text{T}}\gamma_e^2 \frac{B^2}{2} \, ,\tag{15}$$

where $B^2/2$ is the energy density of the Galactic magnetic field, which is not very well determined. A conventional choice is $B \simeq 6\,\mu\mathrm{G}\exp(-|z|/2\,\mathrm{kpc} - r/10\,\mathrm{kpc})$.[39] At the position of the Sun this magnetic field yields a synchrotron loss rate of $b_{\mathrm{syn}} \simeq 4.0 \times 10^{-17}(E_e/\,\mathrm{GeV})^2\,\mathrm{GeV}\,\mathrm{s}^{-1}$.

Note that the interaction between the Galactic magnetic field and dark matter induced electrons and positrons gives rise to synchrotron radiation, which can be probed by radio observations of the Galactic center and halo. In case of decaying dark matter, the resulting limits are weaker, however, than those obtained from local measurements of cosmic rays.[40, 41]

A drastic simplification, which greatly simplifies analytical treatments of the propagation equations, is to assume that the total rate of energy loss is position-independent and can be parametrized as

$$b(E) = \frac{1}{\tau_E}\left(\frac{E}{E_0}\right)^2 ,\tag{16}$$

with $E_0 = 1$ GeV and the time scale $\tau_E \simeq 10^{16}$ s, in accordance with the synchrotron loss rate above. In the relevant energy range, this approximation is good up to factor of about two to three (see e.g. Fig. 1 in Ref. 42).

Rather than measuring the positron flux directly, many experiments measure the positron fraction, which is less susceptible to systematics since most sources of systematic error, such as detector acceptance or trigger efficiency, cancel out when computing the ratio of particle fluxes. The positron fraction is defined as the flux of positrons divided by the total flux of electrons plus positrons, and can be calculated as

$$\mathrm{PF}(E) = \frac{\Phi_{e^+}^{\mathrm{DM}}(E) + \Phi_{e^+}^{\mathrm{bkg}}(E)}{\Phi^{\mathrm{tot}}(E)},\tag{17}$$

where the total electron/positron flux is given by

$$\Phi^{\mathrm{tot}}(E) = \Phi_{e^-}^{\mathrm{DM}}(E) + \Phi_{e^+}^{\mathrm{DM}}(E) + \Phi_{e^-}^{\mathrm{bkg}}(E) + \Phi_{e^+}^{\mathrm{bkg}}(E) ,\tag{18}$$

with $\Phi_{e^\pm}^{\mathrm{DM}}$ and $\Phi_{e^\pm}^{\mathrm{bkg}}$ being the $e^\pm$ fluxes from dark matter decay and the background fluxes, respectively. The background flux of positrons is constituted by secondary positrons produced in the collision of primary cosmic-ray protons and other nuclei with the interstellar medium. On the other hand, the background flux of electrons is constituted by a primary component, presumably produced and accelerated by supernova remnants, as well as a secondary component, produced by spallation of cosmic rays on the interstellar medium and which is much smaller than the primary component. Whereas the spectrum and normalization of secondary electrons and positrons is calculable in a given propagation model (e.g. Ref. 43), the spectrum and normalization of primary electrons is mainly constrained by the direct measurement.
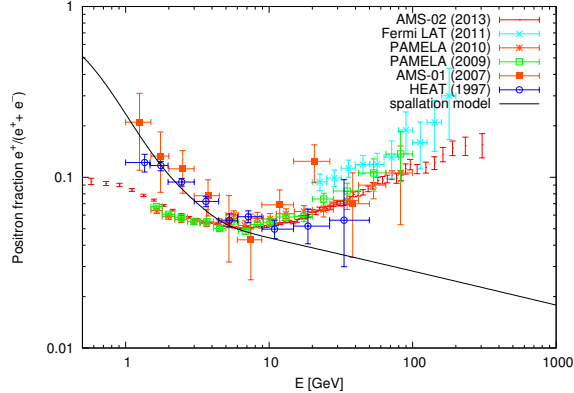
Fig. 1.   Recent observations of the positron fraction by AMS-02,[49] PAMELA,[48,51] Fermi LAT,[52] HEAT.[45] Error bars shown include statistical and systematic errors added in quadrature. Also shown is a representative theoretical exception from production of positrons by cosmic-ray spallation (corresponding to the parametrization in Refs. 58,59). The significant discrepancy between theory and observation at higher energies is evident. The discrepancy at lower energies is due to solar modulation (see Ref. 60).

The possibility of dark matter contributions to the cosmic-ray positron flux has attracted a lot of attention in recent years due to the discovery by a series of increasingly precise cosmic-ray measuments that the positron fraction exhibits a steep rise at energies above 10 GeV. Hints of the existence of this rise had been observed by AMS-01,[44] HEAT[45,46] and CAPRICE.[47] More recently, the existence of this rise was confirmed and measured to high precision by PAMELA[48] and AMS-02.[49] This behavior is in stark contrast with conventional models of positron production by cosmic-ray spallation,[43] which predict that the positron fraction should decrease monotonically with the energy approximately like $\propto E^{-\delta}$ at energies above a few GeV if the primary spectral indices of electrons and positrons at injection are similar.[50] Recent observational results obtained by AMS-02,[49] PAMELA,[48,51] Fermi LAT,[52] AMS-01[44] and HEAT[45] are shown in Fig. 1. Furthermore, recent observations by Fermi LAT have revealed that the combined flux of electrons and positrons up to about 1 TeV roughly follows a smooth power law and is harder than expected from conventional diffusive models.[53] Earlier observations of a spectral feature in the all-electron spectrum by ATIC[54] and PPB-BETS[55] were not confirmed by Fermi LAT. Measurements by the H.E.S.S. telescope[56,57] furthermore indicate that the all-electron spectrum steepens above 1 TeV. Due to the fact that energetic positrons lose energy efficiently through inverse Compton scattering, one can infer that the unknown source of positrons must be local and capable of producing highly energetic cosmic rays.

A number of astrophysical explanations for the positrons excess have been proposed. Models of e^+e^- pair production by the interactions of high-energy photons in the strong magnetic fields of pulsars can reproduce the positron fraction.[61–63]
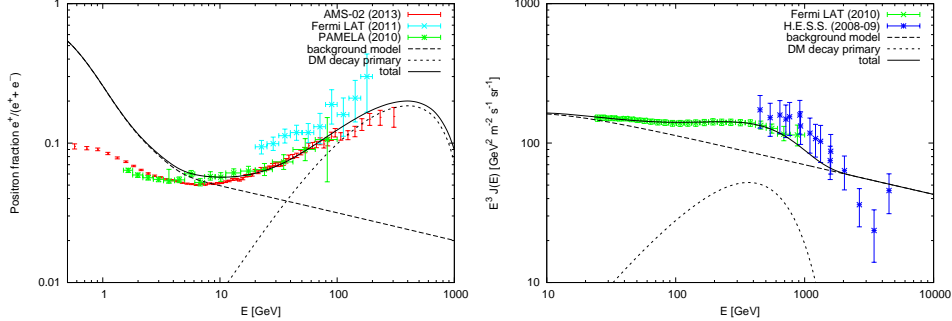
Fig. 2.   *Left panel:* Positron fraction for the decay $\psi_{\mathrm{DM}} \to \mu^+\mu^-\nu$ with $m_{\mathrm{DM}} = 3000$ GeV and $\tau_{\mathrm{DM}} = 1.6 \times 10^{26}$ s. *Right panel:* All-electron flux for the decay $\psi_{\mathrm{DM}} \to \mu^+\mu^-\nu$ with $m_{\mathrm{DM}} = 3000$ GeV and $\tau_{\mathrm{DM}} = 1.6 \times 10^{26}$ s.

Other explanations include a nearby gamma-ray burst,[64] an inhomogeneous cosmic-ray source distribution,[65] the acceleration of secondaries within the sources[66,67] or a nearby supernova explosion.[68]

Many authors have explored the more exotic possibility that the positron excess may be due to dark matter decay into leptonic final states. If the dark matter particles have sufficiently large mass, their decay could produce highly energetic positrons and electrons, which might potentially be the origin of the observed anomalies. Examples of recent works involving decaying dark matter as the source of the positron excess, or use positron data to derive limits upon the decay rate, include Refs. 69–97. Generally, models of dark matter which decays mostly into leptons can provide good fits to the observed lepton abundances provided that the mass of the dark matter is in the range of a few TeV and the lifetime of the dark matter is around $10^{26}-10^{27}$ s. [b] We show a representative example of a fit of a dark matter signal to the cosmic-ray lepton data in the left panel of Fig. 2, where we assume that a dark matter particle of mass $m_{\mathrm{DM}} = 3$ TeV decays via $\psi_{\mathrm{DM}} \to \mu^+\mu^-\nu$ with 100% branching ratio and lifetime $\tau_{\mathrm{DM}} = 1.6 \times 10^{26}$ s. In the right panel of Fig. 2 we display the total electron-plus-positron flux corresponding to the same set of parameters. In Table 3 we list some of the decay modes which yield reasonable agreement with the observed positron fraction and total electron flux, along with the corresponding best-fit values for the dark matter mass and lifetime. Note that with the advent of AMS-02 results, it becomes increasingly difficult to obtain satisfactory fits to the data[95] (the fit can be improved, however, by considering flavor-asymmetric dark matter decays, such as DM $\to \mu^-\tau^{+}$[98,99]).

Generally, decays into leptons will be accompanied by decays into hadrons, photons and neutrinos, which allows for complementary tests of dark matter interpre-

---

[b]Lifetimes of this order exceed the age of the Universe by a factor of $\sim 10^9$, rendering such dark matter particles nearly stable on cosmological timescales.

Table 3. Sample dark matter decay channels that yield a good numerical fit to the positron fraction and the electron flux, together with the best-fit values for the dark matter mass and lifetime. Numbers are taken from Ref. 59.

Decay mode	mass [GeV]	lifetime [10^{26} s]
$\psi_{\rm DM} \to \mu^+\mu^-\nu$	3500	1.1
$\psi_{\rm DM} \to \ell^+\ell^-\nu$	2500	1.5
$\phi_{\rm DM} \to \mu^+\mu^-$	2500	1.8

tations of the positron excess in other indirect detection channels. We discuss these in the following sections.

2.2. *Antiprotons*

Cosmic-ray antiprotons constitute a sensitive probe for exotic – and usually charge-symmetric – contributions from dark matter (with one antiproton measured per 10,000 protons at 1 GeV kinetic energy[100, 101]). Existing models of secondary antiproton production by cosmic-ray spallation match the observed fluxes well, leaving little room for contributions from exotic sources[102, 103] such as dark matter. Thus, antiproton measurements can be used to impose stringent constraints on any dark matter decay modes that involve the production of hadrons.

The general transport equation, Eq. (8), can be simplified for antiprotons by taking into account that in this case energy losses are negligible due to the relatively large proton mass. The transport equation for the antiproton density, $f_{\bar{p}}(T, \vec{r}, t)$ then reads

$$0 = \frac{\partial f_{\bar{p}}}{\partial t} = \vec{\nabla} \cdot (K(T, \vec{r})\vec{\nabla}f_{\bar{p}}) - \vec{\nabla} \cdot (\vec{V_c}(\vec{r})f_{\bar{p}}) - 2h\delta(z)\Gamma_{\rm ann}f_{\bar{p}} + Q(T, \vec{r}) , \quad (19)$$

where the annihilation rate, $\Gamma_{\rm ann}$, is given by

$$\Gamma_{\rm ann} = (n_{\rm H} + 4^{2/3}n_{\rm He})\sigma_{\bar{p}p}^{\rm ann}v_{\bar{p}} . \quad (20)$$

In this expression it has been assumed that the annihilation cross-section between an antiproton and a helium nucleus is related to the annihilation cross-section between an antiproton and a proton by the simple geometrical factor $4^{2/3}$. Furthermore, $n_{\rm H} \sim 1$ cm^{-3} is the number density of Hydrogen nuclei in the Milky Way disk, $n_{\rm He} \sim 0.07\ n_{\rm H}$ the number density of Helium nuclei and $\sigma_{\bar{p}p}^{\rm ann}$ is the proton–antiproton annihilation cross-section, which is parametrized by:[104, 105]

$$\sigma_{\bar{p}p}^{\rm ann}(T) = \begin{cases} 661\ (1 + 0.0115\ T^{-0.774} - 0.948\ T^{0.0151})\ {\rm mbarn}\ , & T < 15.5\ {\rm GeV} \\ 36\ T^{-0.5}\ {\rm mbarn}\ , & T \geq 15.5\ {\rm GeV} \end{cases} \quad (21)$$

The flux of primary antiprotons from dark matter decay is highly sensitive to the choice of propagation parameters, resulting in a variation in the flux as large as two orders of magnitude between the MIN and MAX set of transport parameters. This is due to the fact that theoretical determinations of primary-to-secondary flux
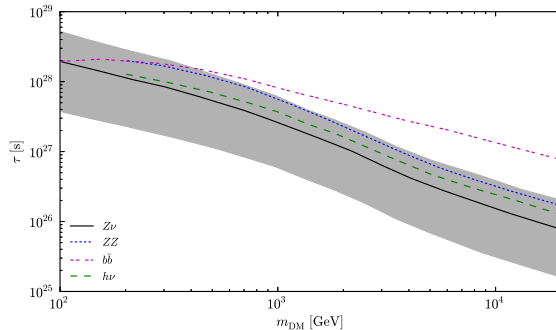
Fig. 3. 95% C.L. lower limits on the dark matter lifetime for decays of fermionic or bosonic dark matter into different final states, derived from *antiproton measurements* by PAMELA in Ref. 106. The gray band indicates for the case of $Z\nu$ final states the uncertainties of the limits, following for the MIN/MED/MAX models as discussed in the text.

ratios suffer from a degeneracy between the diffusion coefficient and the height of the magnetic diffusion zone. For cosmic rays produced in the Galactic disk, very different sets of propagation parameters can yield identical flux ratios. Primary fluxes from dark matter, which are produced everywhere in the dark matter halo and not just in the disk, vary however substantially depending on the portion of the dark matter halo which intersects with the diffusion zone.

Antiproton constraints on decaying dark matter have been computed by a number of authors.[106–108] Constraints derived from the antiproton-to-proton ratio are generally more stringent than those derived from the absolute antiproton flux. We show model-independent constraints from Ref. 106 on various dark matter decay modes in Figs. 3, where the constraints are derived from the requirement that the computed antiproton/proton ratio does not exceed the observed values[100] at 95% C.L. Generally, the resulting constraints on the dark matter lifetime are in tension with the preferred lifetimes for explaining the anomalous leptonic cosmic-ray measurements if the dark matter has significant branching ratios into hadronic final states (cf. Table 3). Improved results on the antiproton flux from AMS-02 can be expected in the very near future.

2.3. *Antideuterons*

The search for antideuterons is a promising method to detect dark matter decays due to the extremely low background fluxes expected from the spallation of cosmic rays on the interstellar medium in the energy range of interest for experimental searches. In fact, all searches for cosmic antideuterons have so far been negative and have only resulted in upper limits on the flux. The best present limit on the cosmic antideuteron flux was set by BESS in the range of kinetic energy per nucleon $0.17 \leq T \leq 1.15\,\mathrm{GeV/n}$, $\Phi_{\bar{d}} < 1.9 \times 10^{-4}\,\mathrm{m}^{-2}\mathrm{s}^{-1}\mathrm{sr}^{-1}(\mathrm{GeV/n})^{-1}$.[109] Interestingly, in the near future the sensitivity of experiments to the cosmic an-

tideuteron flux are expected to increase significantly, namely by more than two orders of magnitude. The Alpha Magnetic Spectrometer (AMS-02) aboard the International Space Station is currently searching for cosmic antideuterons in two energy windows, $0.2 \leq T \leq 0.8$ GeV/n and $2.2 \leq T \leq 4.4$ GeV/n, with an expected flux sensitivity after five years $\Phi_{\bar{d}} = 1 \times 10^{-6} \mathrm{m}^{-2} \mathrm{s}^{-1} \mathrm{sr}^{-1} (\mathrm{GeV/n})^{-1}$ in both energy windows.[110] Furthermore, the balloon-borne General Antiparticle Spectrometer (GAPS) will, starting this decade, undertake a series of flights at high altitude over Antarctica, searching for cosmic antideuterons. In the first phase, a long duration balloon (LDB) flight will search for antideuterons in the range of kinetic energy per nucleon $0.1 \leq T \leq 0.25$ GeV/n with a sensitivity $\Phi_{\bar{d}} = 1.2 \times 10^{-6} \mathrm{m}^{-2} \mathrm{s}^{-1} \mathrm{sr}^{-1} (\mathrm{GeV/n})^{-1}$, while in the second, the ultra long duration balloon (ULDB) flight will search in the range $0.1 \leq T \leq 0.25$ GeV/n with a sensitivity $\Phi_{\bar{d}} = 3.5 \times 10^{-7} \mathrm{m}^{-2} \mathrm{s}^{-1} \mathrm{sr}^{-1} (\mathrm{GeV/n})^{-1}$.[110]

The antideuteron flux expected from spallation of cosmic rays on the interstellar medium is peaked at a kinetic energy per nucleon $T_{\bar{D}} \sim 5$ GeV/n and rapidly decreases at smaller kinetic energies.[111–114] In contrast, the spectrum of antideuterons from dark matter decays is usually much flatter at low kinetic energies and could easily overcome the astrophysical background for sufficiently large decay rates. For this reason, the possibility of detecting antideuterons from dark matter decay has received some attention over the last years.[115, 116]

To describe the antideuteron production it is common to employ the coalescence model,[117–120] which postulates that the probability of the formation of an antideuteron out of an antiproton-antineutron pair with given four-momenta $k_{\bar{p}}^{\mu}$ and $k_{\bar{n}}^{\mu}$ can be approximated as a narrow step function $\Theta \left(\Delta^2 + p_0^2 \right)$, where $\Delta^{\mu} = k_{\bar{p}}^{\mu} - k_{\bar{n}}^{\mu}$ is the difference between the antiproton and antineutron momenta. In this model, the coalescence momentum p_0 is the maximal relative momentum of the two antinucleons that still allows for the formation of an antideuteron. One can show that for $|\vec{k}_{\bar{D}}| \gg p_0$, where $\vec{k}_{\bar{D}} = \vec{k}_{\bar{p}} + \vec{k}_{\bar{n}}$, this ansatz leads to the following differential antideuteron yield in momentum space:

$$\gamma_{\bar{D}} \frac{d^3 N_{\bar{D}}}{d^3 k_{\bar{D}}}(\vec{k}_{\bar{D}}) = \frac{1}{8} \cdot \frac{4}{3} \pi p_0^3 \cdot \gamma_{\bar{p}} \gamma_{\bar{n}} \frac{d^3 N_{\bar{p}} d^3 N_{\bar{n}}}{d^3 k_{\bar{p}} d^3 k_{\bar{n}}} \left(\frac{\vec{k}_{\bar{D}}}{2}, \frac{\vec{k}_{\bar{D}}}{2} \right) , \qquad (22)$$

where the correlation between the antiproton and antineutron production in the hard process has been taken into account. The antideuteron yield can then be calculated using a Monte Carlo event generator and selecting the events which contain an antiproton–antineutron pair produced directly in the hadronization process with a relativistic invariant momentum difference $-\Delta^2 < p_0^2$ (an antiproton produced in a weak decay is separated from an antineutron produced in the hadronization or in other weak decay by a distance much larger than the typical range of the nuclear forces and therefore will not form a bound state). The antideuteron yield can then be calculated in different processes and compared to experimental data to determine the coalescence momentum. As shown in Ref. 116 the coalescence momentum depends on the underlying process and on the center of mass energy. Therefore, the

coalescence momentum inferred from laboratory experiments might differ to the actual one involved in the dark matter decay, thus introducing an important source of uncertainty (note from Eq. (22) that the antideuteron yield scales as p_0^3). This is not the case for the case of decays into weak gauge bosons, since the antideuteron yield from Z boson decay has been measured by ALEPH.[121] From this, following the procedure described above, a coalescence momentum $p_0 = 192 \pm 30$ MeV can be derived.[116]

The propagation of antideuterons in the Milky Way is analogous to the propagation of antiprotons (see Appendix A for details). Since antideuterons are produced by the coalescence of one antiproton and one antineutron, it is apparent that there is a strong correlation between the cosmic antideuteron flux and the cosmic antiproton flux. More concretely, the non-observation of an excess in the PAMELA measurements of the cosmic antiproton-to-proton fraction can be used to set upper limits on the decay width in the channels producing antiprotons, which can then be translated into upper limits on the antideuteron flux in these channels.[116] The corresponding upper limits on the antideuteron flux for the decays into W^+W^- and $b\bar{b}$ are shown in Fig. 4, for $m_{\rm DM} = 200$ GeV and $m_{\rm DM} = 2$ TeV, together with the expected background flux calculated in Ref. 112 (see also Ref. 114) and the sensitivity of future and planned experiments. As apparent from the plot, the upper limits on the hadronic decays set by PAMELA severely constrain the possibility of observing antideuterons from dark matter decay at AMS-02 or GAPS, with the maximum number of expected events being less than one at AMS-02 and one at GAPS, which would not suffice to unequivocally attribute any possible signal to dark matter decays at 95% C.L..[116] Nevertheless, a larger number of events could be observed, and a larger significance of the signal could be achieved, if the upper limit on the decay width into antiprotons is reduced and if the coalescence momentum is enhanced – always under the assumption that the PAMELA limits on an exotic component in the antiproton-to-proton fraction are saturated.[122] Unfortunately, despite the various sources of uncertainty, the observation of an antideuteron flux at AMS-02 or GAPS from dark matter decays seems challenging.

3. Gamma Rays

For dark matter lifetimes of the order 10^{26}–10^{29}s, the high-energetic photons potentially produced by dark matter decay could contribute to the gamma-ray fluxes measured at Earth at an observable level. In the case of hadronic decays, these photons would predominantly come from $\pi^0 \to \gamma\gamma$, whereas the decay into light charged leptons would, e.g., give rise to intense final state radiation. Highly energetic electrons and positrons from dark matter decay can further upscatter photons from the interstellar radiation field (ISRF) into the gamma-ray energy range, and emit bremsstrahlung when interacting with the interstellar medium. For definiteness, we will focus here on gamma-ray energies above 100 MeV.

One general advantage of the gamma-ray channel is the preservation of spec-
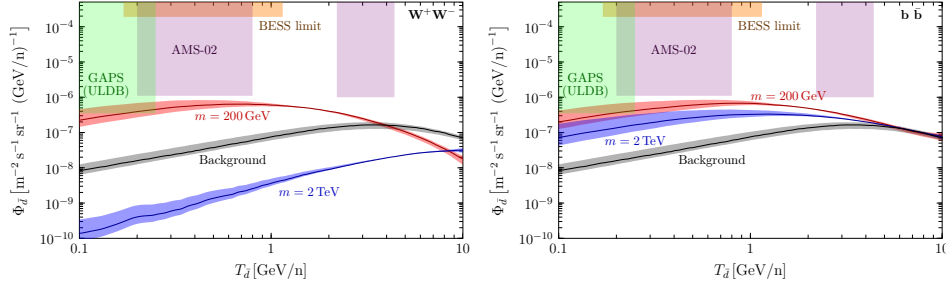
Fig. 4.   Maximum *antideuteron* flux from dark matter decays into W^+W^- (left plot) and $b\bar{b}$ (right plot) compatible with the PAMELA measurements of the antiproton-to-proton fraction for dark matter masses $m_{\mathrm{DM}} = 200$ GeV (red line) and $m_{\mathrm{DM}} = 2$ TeV (blue line) assuming a NFW dark matter halo profile, the MED propagation model and a value of the coalescence momentum $p_0 = 192$ MeV. We also show as a black line the expected background flux calculated in Ref. 112, also for the MED propagation model. The red, blue and grey shaded regions span the propagation uncertainty between MIN, MED and MAX parameters. Plots courtesy of Sebastian Wild.

tral and spatial information (in contrast, antimatter suffers energy losses and undergoes diffusion processes). Though in the case of dark matter annihilation signals, the characteristic signal morphology can greatly help to discriminate signals from backgrounds, for dark matter *decay* signals the most stringent constraints come often from the *isotropic* (and therefore mostly extragalactic) signal component;[123] anisotropies play only a subdominant role.[124] A convincing identification of an isotropic signal would have to rely on distinctive spectral features, such as gamma-ray lines or pronounced bumps or cutoffs from final state radiation. Lastly, predictions for the gamma-ray emission from dark matter decay do not suffer from uncertainties in signal enhancement due to dark matter substructure as in the case of annihilation signals.

We will start with a brief overview of the individual signal contributions, which is followed by a summary of the results of current searches.

3.1. *Signals*

The most relevant contributions to the decay signal are firstly the 'prompt' photons that are directly generated during the decay, and secondly the subsequent inverse Compton emission from the prompt electrons and positrons. We will discuss both components separately.

3.1.1. *Prompt Radiation*

The prompt gamma-ray flux from dark matter decays can be broadly split in a Galactic and an extragalactic component. The differential flux of signal photons
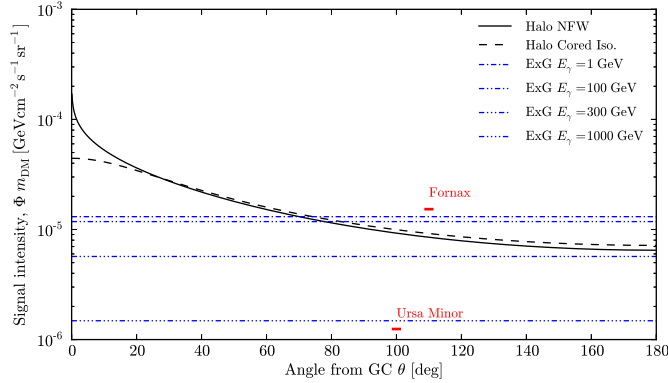
Fig. 5.   Morphology and intensity of the dark matter decay signal. We show the signal intensity as function of the distance towards the Galactic center ψ, assuming a lifetime of $\tau_{\rm DM} = (m_{\rm DM}/{\rm GeV})^{-1}\ 10^{26}\,{\rm s}$ and $\gamma\nu$ final state. The solid and dashed lines correspond to the diffuse Galactic contribution, the dash-dotted line to the extragalactic signal which depends on the emission energy E_γ. For comparison, the signal intensities predicted for the Fornax cluster and the dwarf spheroidal Ursa Minor, both averaged over a region of $1°$ radius, are shown by the red bars.

from our Galaxy is given by

$$\frac{d\Phi_{\rm halo}}{dE_\gamma}(\psi) = \frac{1}{4\pi} \sum_f \frac{\Gamma_f}{m_{\rm DM}} \frac{dN_\gamma^f}{dE_\gamma} \underbrace{\int_0^\infty ds\, \rho_{\rm halo}[r(s,\psi)]}_{\equiv J}\,, \qquad (23)$$

where ψ denotes the angle towards the Galactic center, Γ_f is the decay width corresponding to the final state f, and dN_γ^f/dE_γ is the energy spectrum of photons produced in that channel. Furthermore, $\rho_{\rm halo}(r)$ denotes the density distribution of dark matter particles in our Galaxy as a function of the galactocentric distance $r(s,\psi) = \sqrt{s^2 + R_\odot^2 - 2sR_\odot \cos\psi}$, with $R_\odot = 8.5\,{\rm kpc}$ being the distance of the Sun to the Galactic center, and $\cos\psi = \cos b \cos \ell$, where b and ℓ are the Galactic latitude and longitude, respectively. Commonly adopted density profiles $\rho_{\rm halo}$ were discussed in Section 1.

For the case of a NFW (cored isothermal) profile, the predicted dark matter signal flux from the Galactic halo as function of ψ is shown by the solid (dashed) line in Fig. 5. For definiteness, we assume a dark matter lifetime of $\tau_{\rm DM} = (m_{\rm DM}/{\rm GeV})^{-1}\ 10^{26}\,{\rm s}$, and 100% annihilation into a $\gamma\nu$ final state. The difference between the two profiles becomes substantial at angles $\psi \lesssim 20°$ close to the Galactic center, and leads to signal predictions that differ by a factor of four and more at $\psi \lesssim 0.1°$. At larger values of ψ the main uncertainty is the overall normalization of ρ_{halo}.

The extragalactic contribution to the gamma-ray signal is generated by the decay of dark matter particles at cosmological distances. It is largely isotropic and affected by the redshift as well as as the finite optical depth of the Universe. The

differential flux is given by

$$\frac{d\Phi_{\mathrm{eg}}}{dE_\gamma} = \frac{1}{4\pi}\frac{\Omega_{\mathrm{DM}}\rho_{\mathrm{c}}}{m_{\mathrm{DM}}}\int_0^\infty dz \sum_f \Gamma_f \frac{1}{H(z)}\frac{dN_\gamma^f}{dE_\gamma}\left[(z+1)E_\gamma\right]\, e^{-\tau(E_\gamma,z)}\,. \qquad (24)$$

Here, $\rho_{\mathrm{c}} = 4.9 \times 10^{-6}\,\mathrm{GeV\,cm^{-3}}$ denotes the critical density of the Universe, and $H(z) = H_0\sqrt{\Omega_\Lambda + \Omega_{\mathrm{m}}(z+1)^3}$ is the Hubble rate as a function of redshift z.[c] With the factor $e^{-\tau}$, we incorporate attenuation effects due to pair-production and – in the TeV regime – photon-photon scattering on the intergalactic background light (IBL). The attenuation factor is determined by the optical depth $\tau(E_\gamma, z)$, for which we adopt the results from Ref. 12. These results are based on the AEGIS multi-wavelength analysis presented in Ref. 125, and compatible with recent HESS[126] and Fermi[127] observations.

In Fig. 5 the horizontal lines show the isotropic flux of extragalactic gamma rays for different energies E_γ of the prompt photons (as above, we integrate over all gamma-ray energies to calculate the flux). For our reference Galactic dark matter halo and photon energies below about 100 GeV, the extragalactic dominates the Galactic signal at angles $\psi \gtrsim 90°$. At these energies, half of the extragalactic signal stems from redshifts $z \gtrsim 0.8$. However, at higher energies the attenuation effects start to suppress the extragalactic signal, and at $\gtrsim 800$ TeV energies only the local Universe ($z \lesssim 0.1$) remains observable in gamma rays.

Besides the Galactic and cosmological components, massive nearby dark matter halos – such as galaxy clusters or Milky Way satellite galaxies – contribute to the overall signal (cf. Ref. 128). They appear as point-like or marginally extended objects and could be used to identify a signal above the diffuse background. The corresponding signal flux can be calculated as shown in Eq. (23), with the substitutions $\rho_{\mathrm{halo}} \to \rho_{\mathrm{src}}$ and $R_\odot \to D$; ρ_{src} is the dark matter distribution of the target and D its distance to the Earth. In Fig. 5, we show for two interesting targets – the dwarf spheroidal Ursa Minor and the galaxy cluster Fornax – the associated fluxes averaged over a region with a radius of $1°$ (we adopt here values from Ref. 129). The predicted signal from these and other targets is at most marginally more intense (and in most cases weaker) than the diffuse Galactic and extragalactic signal components.

3.1.2. *Inverse Compton Scattering*

High-energetic electrons and positrons that are produced during the decay of dark matter particles can upscatter photons from the interstellar radiation field (ISRF) to gamma-ray energies via inverse Compton scattering.[130] Besides the CMB, the ISRF includes thermal dust radiation as well as diffuse starlight.[38] We will here

---

[c]We adopt the parameters $\Omega_\Lambda = 0.69$, $\Omega_{\mathrm{m}} = 0.31$, $\Omega_{\mathrm{DM}} = 0.26$ and $h \equiv H_0/100\,\mathrm{km\,s^{-1}\,Mpc^{-1}} = 0.68$, as derived from Planck+WP+highL+BAO data (see Ref. 9).

briefly review the calculation of the Galactic ICS signal, and refer to Refs. 59, 131 for the extragalactic counterpart.

The differential production rate of gamma rays with energies around E_γ at position $\vec{r}$ by the inverse Compton scattering of highly energetic electrons and positrons on photons of the ISRF reads

$$\frac{dR_\gamma^{\text{IC}}(\vec{r})}{dE_\gamma} = \int_0^\infty d\epsilon \int_{m_e}^\infty dE_e \, \frac{d\sigma^{\text{IC}}(E_e, \epsilon)}{dE_\gamma} f_{e^\pm}(E_e, \vec{r}) f_{\text{ISRF}}(\epsilon, \vec{r}) \ . \qquad (25)$$

Here, the differential number density of electrons (or positrons) from dark matter decay is given by $f_{e^\pm}(E_e, \vec{r})$, and the differential number density of the ISRF is $f_{\text{ISRF}}(\epsilon, \vec{r})$. Furthermore, $d\sigma^{\text{IC}}/dE_\gamma(E_e, \epsilon)$ is the differential ICS cross section for an electron with energy E_e to up-scatter ISRF photons from ϵ to E_γ. It follows from the Klein-Nishina formula and is given by

$$\frac{d\sigma^{\text{IC}}(E_e, \epsilon)}{dE_\gamma} = \frac{3}{4} \frac{\sigma_{\text{T}}}{\gamma_e^2 \, \epsilon} \left[2q \ln q + 1 + q - 2q^2 + \frac{1}{2} \frac{(q\Gamma)^2}{1 + q\Gamma}(1 - q) \right], \qquad (26)$$

where $\sigma_{\text{T}} = 0.67$ barn denotes the Compton scattering cross section in the Thomson limit, $\gamma_e \equiv E_e/m_e$ is the Lorentz factor of the electron, $m_e = 511\,\text{keV}$ is the electron mass, and we defined the quantities $\Gamma \equiv 4\gamma_e \epsilon/m_e$ and $q \equiv E_\gamma/\Gamma(E_e - E_\gamma)$. Eq. (26) holds in the limit where $\epsilon, m_e \ll E_e$, and kinematics and the neglect of down-scattering require that $\epsilon \leq E_\gamma \leq (1/E_e + 1/4\gamma_e^2 \epsilon)^{-1} \equiv E_\gamma^{\max}$. In case of CMB photons with $\epsilon \sim 2.4 \times 10^{-4}\,\text{eV}$, ICS photons are produced up to energies of $E_\gamma \sim 3.7\,\text{GeV}\, E_{\text{TeV},e}^2$, with electron energies given in units of TeV.

The number density of electrons and positrons from dark matter decays, $f_{e^\pm}(E_e, \vec{r})$, follows from solving the full transport equation Eq.(8). At energies above a few tens of GeV, energy losses dominate, which allows some approximate, simple analytical solutions (see e.g. discussion in Ref. 124). A commonly adopted model for the ISRF is the one in Ref. 38. Using these distributions and Eq. (25), the gamma-ray flux from ICS that is received at Earth as function of Galactic longitude ℓ and latitude b is given by

$$\frac{d\Phi_{\text{halo,IC}}}{dE_\gamma}(\ell, b) = 2 \cdot \frac{1}{4\pi} \int_0^\infty ds \, \frac{dR_\gamma^{\text{IC}}[r(s, \ell, b)]}{dE_\gamma} \ , \qquad (27)$$

where the factor of 2 takes into account the fact that both dark matter electrons and positrons contribute equally to the total flux of gamma rays.

Starlight is brightest towards the Galactic center; together with the geometry of the Galactic cosmic-ray diffusion zone this causes the ICS dark matter signal to be elongated and aligned with the Galactic plane – in contrast to the approximately spherical prompt component of the signal, making it potentially difficult to discriminate from an ICS signal from dark matter annihilation.[132] However, due to the large Galactic foregrounds in direction of the Galactic center it is more efficient to search for the signal at the Galactic poles. There, the predicted signal intensity depends critically on the electrons and positrons that are generated by dark matter decay inside the Galactic halo, but *outside* of the diffusion zone.
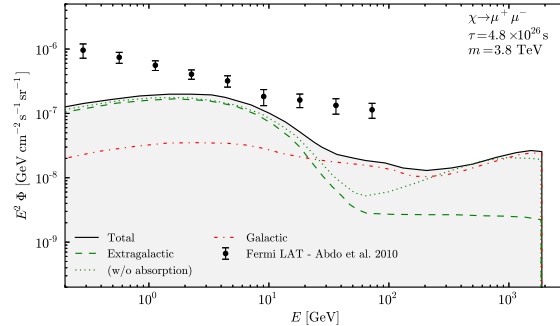
Fig. 6.   The extragalactic gamma-ray background as measured by the Fermi LAT,[133, 134] compared to exemplary predictions for decay into $\mu^+\mu^-$ final states. The dashed (dotted) line shows the extragalactic contribution with (without) absorption effects included; the dash-dotted line is the Galactic contribution. Fluxes are taken from Ref. 135 and correspond to the flux predictions for the direction $\ell = 180°$ and $b = 0°$ (see text details); ICS emission dominates at energies below ~ 60 GeV.

Search strategies for dark matter signals often build upon specific morphological and spectral signal characteristics and depend on the dark matter model at hand. For decaying dark matter with masses in the GeV–TeV regime, the most relevant targets are the isotropic gamma-ray background (IGBG), the Galactic halo, galaxy clusters, and sharp spectral signatures.

3.1.3. *Morphological Features*

As shown in Fig. 5, at angles of a few tens of degrees with respect to the Galactic center, the dark matter decay signal is most intense and the vast majority of signal photons would come from the Galactic halo itself. Unfortunately, the Galactic center is also the region with the largest foregrounds at GeV energies. Thus, for decaying dark matter signals, the best regions of interest lie offset from the Galactic Center, above or below the Galactic plane.[123, 124] In fact, it turns out that measurements of the IGBG, which dominates the diffuse emission observed in direction of the Galactic poles, provide some of the most stringent constraints on dark matter decay.

Technically, the IGBG is the – by construction – isotropic flux that remains after subtracting the Galactic diffuse emission and known point sources. The IGBG was recently determined by Fermi LAT up to energies of 100 GeV,[133] preliminary results up to 400 and 580 GeV were presented in Refs. 134, 136. The measured fluxes are shown in Fig. 6, together with an exemplary dark matter signal. The IGBG is usually attributed to gamma rays originating from outside of our Galaxy, and thought to be made up entirely by unresolved point-like sources, like blazars, millisecond pulsars or star- forming galaxies (see Ref. 137 and references therein).

As discussed above, dark matter decay at cosmological distances would generate a nearly isotropic gamma-ray signal, which would entirely contribute to the IGBG.
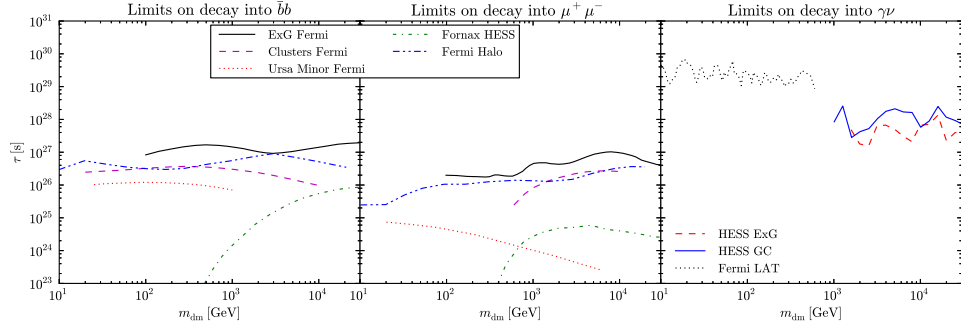
Fig. 7. Summary of 95%CL lower limits on the dark matter lifetime, derived from gamma-ray observations, assuming different final states: *left panel:* $\psi \to \bar{b}b$, *central panel:* $\psi \to \mu^+\mu^-$ and *right panel:* $\psi \to \nu\gamma$. Limits are taken from Refs. 129, 135, 138, 139 in case of $\bar{b}b$ and $\mu^+\mu^-$ final states, and from Refs. 140, 141 in case of gamma-ray lines.

However, close to the Galactic poles the angular dependence of the Galactic signal is in case of dark matter decay relatively weak, such that this part of the Galactic signal would be likely misidentified as being extragalactic. As a very conservative lower limit on the dark matter signal flux contribution to the IGBG, one can adopt the signal strength in direction of the anti-center, namely $\Phi_{eg} + \Phi_{halo}(\psi = 180°)$.

3.2. *Targets and Searches*

For a decaying dark matter signal, a simple but very robust constraint can be derived from the requirement that the dark matter signal should not significantly exceed the measured IGBG; this approach was used by many groups.[42, 59, 135, 142–146] More realistic constraints can be obtained by a subtraction of astrophysical contributions,[137, 147] or by a detailed spectral analysis.[135, 148] The results from Ref. 135 – based on a spectral fit to the IGBG with the background modeled as power-law – are shown in Fig. 7. They are stronger than the limits obtained by the 'robust' method by a factor of up to five.[135]

Although, as outlined above, the monopole of the dark matter decay signal turns out to be the most effective observable, the dipole anisotropy towards the Galactic center can also have important effects [we define the dipole anisotropy here as $A = (J_{|\ell| \leq 90°} - J_{|\ell| > 90°})/(J_{|\ell| \leq 90°} + J_{|\ell| > 90°})$]. At higher latitudes (masking $|b| < 10°$), this anisotropy is of the order $A = 20\%$–36%,[124] depending on the profile of the Galactic dark matter halo and the gamma-ray energy. It can potentially be useful to finally discriminate a decay signal from the (truly isotropic) astrophysical extragalactic gamma-ray background, since the observation of spectral features in the dipole anisotropy as function of energy could indicate a dark matter signal that dominates over a short energy range.[124] Unfortunately, the recently discovered Fermi Bubbles[149, 150] contribute significantly to the dipole anisotropy at higher latitudes, which complicates the extraction of a clear dark matter induced dipole signal.

In regions closer to the Galactic Center (which might be actually favorable in case of ICS signals[42]), an analysis of the diffuse gamma-ray emission requires a careful modeling of the Galactic diffuse and point-source emission. Conservative upper limits on the decay width can always be obtained by requiring that the observed fluxes are not exceeded significantly.[143,144] Limits that result from attempting a subtraction of Galactic emission have been derived in Ref. 42 using a simple reference model for the Galactic emission, and in Ref. 139 employing a detailed fit to the gamma-ray data. The region of interest used in Ref. 139, $5° < |b| < 15°$ and $|\ell| < 80°$, spans a large part of the sky above and below the Galactic disk. The gamma-ray flux from this region was fitted with a model for the Galactic emission while marginalizing over a large number of parameters that describe amongst others the details of CR diffusion and source distributions, the Galactic magnetic field and uncertainties in the interstellar medium. In the energy range 0.1–300 GeV no residual emission was found after subtraction of the best-fit model. The resulting limits on an additional dark matter signal are quite competitive and shown in Fig. 7 as dash-dot-dotted lines (3σ limits). In case of $\bar{b}b$ final states, they are comparable to the results obtained from Galaxy cluster observations, which will be discussed next. For $\mu^+\mu^-$ final states, starlight leads to a strong ICS signal even for dark matter masses considerably below 1 TeV, where the cluster limits become very poor.

Nearby galaxy clusters that are interesting for dark matter searches have a typical angular scale of $\mathcal{O}(1°)$ in the sky, with a signal profile that increases steeply towards their center and with peak intensities much higher than the Galactic signal. However, when taking into account finite angular resolution and statistics of instruments like the Fermi LAT, the maximum signal intensities are comparable to or smaller than the Galactic halo signal. This is shown in Fig. 5 for the Fornax clusters, which is one of the brightest targets (intensities are averaged over a region of 1° radius).

The gamma-ray signal from dark matter decaying in nearby galaxy clusters would be extended enough to be seen as an marginally extended source by Fermi LAT. Refs. 129, 138 searched for such emission in up to eight clusters using Fermi LAT data (see also Refs. 123, 135, 151–154). No signal was found, and upper limits were derived on the decay rate by merging the likelihood functions of the different observations into a combined likelihood that also takes into account cluster mass uncertainties associated with the underlying X-ray measurements.[138] For the cases of decay into $\bar{b}b$ and $\mu^+\mu^-$ final states, we show the limits in Fig. 7. Note that conservatively only ICS on the CMB has been taken into account when calculating the limits. They turn out to be weaker than the limits obtained from the IGBG, but are still strong enough to be in mild tension with the decaying dark matter explanation of the positron excess observed by PAMELA and AMS-02 (see discussion above). For comparison, we also show the limits that were derived from HESS observations of the Fornax cluster. In the energy range of interest, these limits are hardly competitive.[135]

Other targets considered in the literature include dwarf spheroidal galaxies (as illustrative example Ursa Minor is shown in Fig. 5)[123, 129, 155, 156] and the angular power spectrum,[124] but the corresponding constraints are significantly weaker than the ones derived from the IGBG.

3.2.1. *Spectral Features*

As discussed above, the most constraining gamma-ray observable for decaying dark matter at GeV–TeV energies is the IGBG. One clear disadvantage of the IGBG is the absence of any strong morphological feature that could help to discriminate a dark matter signal from other astrophysical sources (though the dipole-anisotropy due to our off-center position in the halo might help[123, 124]). However, the IGBG can be measured in a very large fraction of the sky away from the Galactic disc. As a consequence, in contrast to many other observables, the statistical error of the flux is typically extremely small. This turns the IGBG into an excellent target to search for specific *spectral* signatures as smoking gun signals for dark matter decay.

The most prominent spectral signature would be a gamma-ray line from two-body decays into photons or photon pairs. If both final state particles are approximately massless, as e.g. in $\psi \to \gamma\nu$, the gamma-ray line is observed at an energy of half the dark matter mass, $E_\gamma = m_{\mathrm{DM}}/2$. Such gamma-ray lines are often present as one-loop corrections to the main decay channel,[151] and typically significantly suppressed. Among the theoretical decaying dark matter scenarios that actually predict the emission of *strong* lines are gravitino dark matter with a mild violation of R-parity[157] or hidden sector dark matter decaying via higher-dimensional operators.[90] We will discuss these models below in Section 5.

A closely related spectral signature are the box-shaped spectra that are produced in cascade decays like $\psi \to \phi\phi$, with a subsequent $\phi \to \gamma\gamma$.[158] The corresponding gamma-ray spectrum has step-like edges, $dN_\gamma/dE \propto \theta(E^+ - E)\theta(E - E^-)$, where the $E^\pm$ are functions of m_{DM} and m_ϕ.[158] In the limit $m_\phi \to m_{\mathrm{DM}}$, the signal approaches a monochromatic line at an energy $E_\gamma = m_{\mathrm{DM}}/4$.

Different groups have explicitly searched for these signatures, using Fermi LAT[140, 159–163] and HESS[141, 151] data. No indication for a signature that could be attributed to decaying dark matter was found. (The 130 GeV feature at the Galactic center tentatively observed by the Fermi LAT[140, 161, 162, 164, 165] can be interpreted as a signal from dark matter decay,[166, 167] but its spatial profile strongly disfavors this possibility.[25])

At gamma-ray energies 5–300 GeV, the strongest limits come from Fermi LAT[140] (limits down to 1 GeV were derived in Ref. 160). These limits are based on nearly all-sky observations, excluding only the Galactic discs with its large foregrounds. As shown in Fig. 7, they are stronger than limits on purely hadronic and leptonic final states by two to three orders of magnitude. Above 500 GeV and up to 25 TeV, the best limits on gamma-ray lines come from HESS. Ref. 141 presented flux upper limits from a spectral analysis of the IGBG as well as the Galactic center. We

translate these limits into upper limits on the branching width into $\gamma\nu$ final states, see Fig. 7 (right panel). They essentially extend the strong results from Fermi LAT to higher energies, though at a somewhat lower level. Fermi LAT limits on box-shaped spectra were derived Ref. 158. Next-generation instruments like CTA and GAMMA-400 are expected to improve the limits on gamma-ray lines by up to an order of magnitude within the upcoming ten years or so.[168]

4. Neutrinos

The calculation of the neutrino flux from dark matter decays proceeds along similar lines as for gamma-rays, with the fluxes being analogous to those given by Eqs.(23,24). Namely,

$$\frac{d\Phi_{\text{halo}}}{dE_\nu}(\psi) = \frac{1}{4\pi} \sum_f \frac{\Gamma_f}{m_{\text{DM}}} \frac{dN_\nu^f}{dE_\nu} \int_0^\infty \rho_{\text{halo}}[r(s,\psi)]ds \tag{28}$$

for the decay of dark matter particles in the Milky Way halo, and

$$\frac{d\Phi_{\text{eg}}}{dE_\nu} = \frac{1}{4\pi} \frac{\Omega_{\text{DM}}\rho_c}{m_{\text{DM}}} \int_0^\infty dz \frac{1}{H(z)} \sum_f \Gamma_f \frac{dN_\nu^f}{dE_\nu}[(z+1)E_\nu] \tag{29}$$

for the redshifted contribution from dark matter decays at cosmological distances. Note that for GeV-TeV dark matter masses, and in contrast to gamma-rays, neutrinos are not significantly absorbed while they propagate to the Earth.

After being produced in the decay of dark matter particles, neutrinos undergo flavor oscillations. Neglecting CP violating effects during propagation and taking the best fit values of the neutrino oscillation parameters $\sin^2\theta_{12} = 0.30$, $\sin^2\theta_{23} = 0.41$, $\sin^2\theta_{13} = 0.023$,[169] the conversion probabilities read:

$$P(\nu_e \leftrightarrow \nu_e) = 0.56\,, P(\nu_e \leftrightarrow \nu_\mu) = 0.28\,,$$
$$P(\nu_e \leftrightarrow \nu_\tau) = 0.16\,, P(\nu_\mu \leftrightarrow \nu_\mu) = 0.34\,, \tag{30}$$
$$P(\nu_\mu \leftrightarrow \nu_\tau) = 0.37\,, P(\nu_\tau \leftrightarrow \nu_\tau) = 0.46\,.$$

Thus, a primary neutrino flux in a specific flavor is redistributed almost equally into all neutrino flavors during propagation and any flavor information is lost.

The neutrino spectrum from dark matter decay depends on the concrete decay channel. The simplest possibility for dark matter decay, and which arises in many well motivated models, is the direct decay into two neutrinos, for a scalar particle, or into $\gamma\nu$, for a fermion. In this case, the resulting spectrum consists of a monochromatic line and an integral of the redshifted line from the extragalactic signal. In the case of decays into $(Z^0, h)\nu$, in addition to this signal there is also a continuum of neutrinos produced in the decay and fragmentation of the Z^0 and Higgs bosons. Another simple channel is the three body decay into electrons, $\psi \to e^+e^-\nu$ which in the most common scenarios (namely when the decay is mediated by a heavy scalar or a heavy vector boson) has the familiar triangular shape when plotted in a logarithmic axis. Lastly, decay modes into other particles particles which eventually
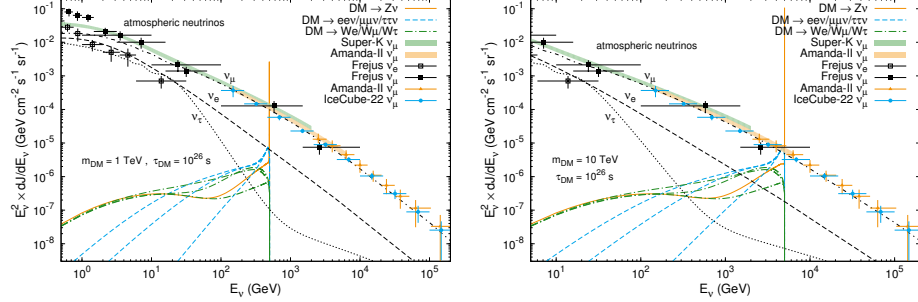
Fig. 8. Neutrino spectra for different decay channels of a fermionic dark matter candidate. From Ref. 179. See text for details.

produce neutrinos in their decay or fragmentation (such as muons, taus, or weak gauge bosons) generate a softer neutrino energy spectrum.

The most important background for the detection of a neutrino flux from dark matter decays comes from neutrinos produced in cosmic-ray interactions with the Earth's atmosphere, and which have a flux that was calculated in Ref. 170. Other sources of background are tau neutrinos from the decay of charmed particles that are also produced in cosmic-ray collisions with the atmosphere,[171] neutrinos produced in cosmic-ray interactions with the solar corona[172] and neutrinos produced in cosmic-ray interactions with the interstellar medium in the Milky Way.[173]

The neutrino spectra at the Earth from various decay modes are shown for the case of a fermionic dark matter particle in Fig. 8, fixing for concreteness the dark matter mass to 1 TeV or 10 TeV and the lifetime to $\tau_{\rm DM} = 10^{26}$ s, which is the reference value quoted in Eq. (1). The spectra include both the contribution from dark matter decays in the halo as well as the redshifted contribution from decays at cosmological distances. The plot also shows the expected atmospheric background and the data measured by the Fréjus,[174] Super-Kamiokande,[175] AMANDA-II[176] and IceCube[177, 178] experiments. As apparent form the plot, the predicted flux from dark matter decay lies considerably below the measured muon neutrino flux. Therefore, detecting a dark matter signal requires an efficient suppression of the backgrounds. As argued in Ref. 179 this could be achieved by considering neutrinos arriving from all directions in the sky, since this choice optimizes the significance of the signal, and by exploiting the spectral information carried by the neutrinos produced in the dark matter decay.

Several groups have searched for signals of dark matter decays in neutrino telescopes.[179–184] No signal has been observed, thus implying lower limits on the dark matter lifetime from the Super-Kamiokande data or the IceCube data, which are shown in Fig. 9 for various decay channels. The search for neutrinos from dark matter decay has been extended to heavier dark matter masses in Refs. 185, 186, finding lower limits for the lifetime of $\mathcal{O}(10^{26} - 10^{28})$ s for masses between 10 TeV and the Grand Unification scale.
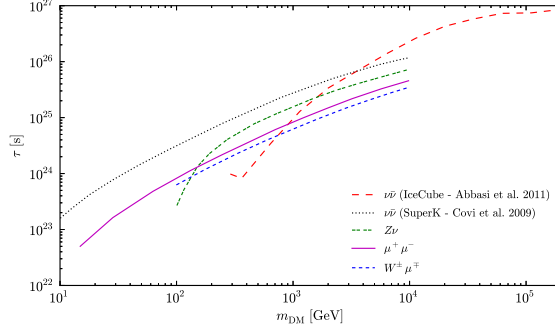
Fig. 9.   90% C.L. exclusion region in the lifetime vs. mass plane for a decaying dark matter candidate from the non-observation of an excess in the Super-K data (from Ref. 179) and IceCube (from Ref. 184).

5. Models

5.1. *Lagrangian Analysis*

Before presenting some concrete models containing unstable dark matter candidates, we will first introduce generic Lagrangians leading to the decay of the dark matter particles.[151, 185, 187] Let us first discuss the scenario where the dark matter particle is a scalar. In this case the effective Lagrangian that induces the decay $\phi_{\mathrm{DM}} \to f\bar{f}$ contains a dimension 4 operator:

$$- \mathcal{L}_{\mathrm{eff}} = y\phi_{\mathrm{DM}}\bar{f}f + \mathrm{h.c.} \tag{31}$$

where y is the coupling constant. The decay rate can be straightforwardly calculated, the result being:

$$\Gamma(\phi_{\mathrm{DM}} \to f\bar{f}) = \frac{|y|^2 N_c}{8\pi}m_{\mathrm{DM}} \ . \tag{32}$$

where N_c is a color factor. For $N_c = 1$ the lifetime is

$$\tau_{\mathrm{DM}} \simeq 2 \times 10^{26}\,\mathrm{s} \left(\frac{y}{10^{-26}}\right)^{-2} \left(\frac{m_{\mathrm{DM}}}{1\,\mathrm{TeV}}\right)^{-1} \ . \tag{33}$$

Therefore, present cosmic rays measurements require a very large suppression of the effective coupling if the dark matter particle is a scalar which decays into a fermion–antifermion pair. A similar conclusion applies to a vector dark matter particle that decays into a fermion–antifermion pair.

   If the dark matter particle is a spin-1/2 fermion, the decays are necessarily induced by higher dimensional effective operators generated by dark matter interactions with heavy scalars or heavy vectors. A general discussion of the possible three-body decays can be found in Ref. 151. For example, the dark matter decay $\psi \to f\bar{f}\nu$ can be induced by the following Lagrangian involving the heavy scalar Σ:

$$\mathcal{L}_{\mathrm{eff}}^{\Sigma} = -\bar{\psi}_{\mathrm{DM}} \left[\lambda_{f\psi}^L P_L + \lambda_{f\psi}^R P_R\right] f\,\Sigma^{\dagger} - \bar{\nu}\lambda_{fN}^R P_R f\,\Sigma^{\dagger} + \mathrm{h.c.} \ , \tag{34}$$

where $P_L = (1 - \gamma^5)/2$ and $P_R = (1 + \gamma^5)/2$ are the left- and right-handed chirality projectors, respectively. In this case, the dark matter decay width is given by:

$$\Gamma(\psi_{\text{DM}} \to f\bar{f}\nu) = \frac{|\lambda_{\text{eff}}|^4 N_c}{3072\pi^3} \frac{m_{\text{DM}}^5}{M_\Sigma^4} \,, \tag{35}$$

where $|\lambda_{\text{eff}}|^4 = (|\lambda_{f\psi}^R|^2 + |\lambda_{f\psi}^L|^2)|\lambda_{f\nu}^R|^2$ and N_c is a color factor. In contrast, if the decay is mediated by a charged vector, the effective Lagrangian reads[d]

$$\mathcal{L}_{\text{eff}}^V = -\bar{\psi}_{\text{DM}}\gamma^\mu \left[\lambda_{f\psi}^L P_L + \lambda_{f\psi}^R P_R\right] f \, V_\mu^\dagger - \bar{\nu}\gamma^\mu \lambda_{fN}^R P_R f \, V_\mu^\dagger + \text{h.c.} \,. \tag{36}$$

In this case the decay width is:

$$\Gamma(\psi_{\text{DM}} \to f\bar{f}\nu) = \frac{|\lambda_{\text{eff}}|^4 N_c}{768\pi^3} \frac{m_{\text{DM}}^5}{M_V^4} \,, \tag{37}$$

where, again, $|\lambda_{\text{eff}}|^4 = (|\lambda_{f\psi}^R|^2 + |\lambda_{f\psi}^L|^2)|\lambda_{f\nu}^R|^2$ and N_c is a color factor. Note that the decay width for the decay mediated by a vector is a factor of four larger than the one mediated by a scalar, under the assumption that $M_V = M_\Sigma$ in Eqs. (35) and (37). In the case that the decay is mediated by a heavy scalar, the lifetime reads, for $N_c = 1$,

$$\tau_{\text{DM}} \simeq 6 \times 10^{25}\,\text{s} \left(\frac{|\lambda_{\text{eff}}|}{1}\right)^{-4} \left(\frac{M_\Sigma}{10^{15}\,\text{GeV}}\right)^4 \left(\frac{m_{\text{DM}}}{1\,\text{TeV}}\right)^{-5} \,, \tag{38}$$

while in the case that the decay is mediated by a heavy vector the lifetime is a factor of four smaller. As apparent from this formula, the longevity of the dark matter particle requires either very large masses for the mediators ($M_\Sigma \gtrsim 10^{15}$ GeV for $|\lambda_{\text{eff}}| \sim 1$ and $m_{\text{DM}} \sim 1\,\text{TeV}$) and/or very small couplings in the interaction ($|\lambda_{\text{eff}}| \lesssim 10^{-12}$ for $M_\Sigma \sim 2\,\text{TeV}$ and $m_{\text{DM}} \sim 1\,\text{TeV}$).

Particularly interesting are those Lagrangians leading to the two-body decay of the dark matter particle into one or two photons, namely $\phi \to \gamma\gamma$, γZ or γh for scalar particles and $\psi \to \gamma\nu$ for spin 1/2 particles. There are many possibilities for the effective interactions that induce the decay (see Ref. 187 for a comprehensive discussion). For example, the decay of a spin 1/2 dark matter particle $\psi \to \nu\gamma$ can be induced by the following effective Lagrangian[185, 187, 188]

$$\mathcal{L} = \frac{1}{2}\bar{\psi}_{\text{DM}}\,\sigma_{\alpha\beta}(\mu + \epsilon\gamma_5)\,\nu F^{\alpha\beta} + \text{h.c.} \tag{39}$$

where $F^{\alpha\beta}$ is the electromagnetic field strength tensor, while μ and ϵ are the magnetic and electric transition moments, respectively. If the dark matter and the neutrino have the same CP parities, the magnetic transition moment vanishes, while when they have opposite CP parities, the electric transition moment vanishes. In either case, the decay rate can be cast as

$$\Gamma(\psi_{\text{DM}} \to \nu\gamma) = \frac{|\mu_{\text{eff}}|^2}{8\pi} m_{\text{DM}}^3 \,, \tag{40}$$

---

[d]We assume here that the decay is dominated by the charged-current interaction; in more generality the decay could also be mediated by a neutral current interaction.

where we have defined an effective neutrino magnetic moment, $|\mu_{\rm eff}| \equiv \sqrt{|\mu|^2 + |\epsilon|^2}$. The corresponding lifetime reads in this case:

$$\tau_{\rm DM} \simeq 2 \times 10^{26}\,{\rm s} \left(\frac{|\mu_{\rm eff}|}{10^{-29}\,{\rm GeV}^{-1}}\right)^{-2} \left(\frac{m_{\rm DM}}{1\,{\rm TeV}}\right)^{-3} , \qquad (41)$$

which requires a very suppressed effective magnetic moment in order to obey the strong limits on the dark matter lifetime from gamma-ray line searches.

In specific models, the effective Lagrangian Eq. (39) is generated by quantum effects. Concretely, the Lagrangians, Eqs. (34,36) generate such a magnetic moment, which can be parametrized as:[151]

$$|\mu_{\rm eff}| = \frac{q\,m_{\rm DM}\,|\theta_{\rm eff}|^2}{64\pi^2 M_\Sigma^2} , \qquad (42)$$

where q is the electric charge of the fermion, M_Σ is the mass of the heavy scalar particle and $\theta_{\rm eff}$ is a combination of the couplings of the dark matter particle and the neutrino to the heavy scalar in the loop. In this case, the lifetime reads:

$$\tau_{\rm DM} \simeq 7 \times 10^{28}\,{\rm s} \left(\frac{\theta_{\rm eff}}{1}\right)^{-4} \left(\frac{M_\Sigma}{10^{15}\,{\rm GeV}}\right)^4 \left(\frac{m_{\rm DM}}{1\,{\rm TeV}}\right)^{-5} . \qquad (43)$$

The decay $\psi \to \gamma\nu$ generated radiatively by the Lagrangians, Eqs. (34,36) has a width which is about two-three orders of magnitude smaller than the width of the tree level, three-body decay $\psi \to f\bar{f}\gamma$ (see eq.38). However, the suppressed decay rate could be compensated by the stronger limits on this channel from gamma-line searches. In fact, as as shown in Ref. 151, in some scenarios the limits from searches for gamma-ray lines can be competitive with the limits from electron/positron measurements (and, interestingly, without suffering from propagation uncertainties). Future instruments, such as the Cerenkov Telescope Array[189] will offer complementary limits on this class of scenarios. One can follow a similar reasoning for scenarios where the dark matter decays into a quark–antiquark pair and a neutrino. An analysis comparing the limits on the parameter space from gamma-ray lines and from the non-observation of a significant excess in the PAMELA measurements of antiproton-to-proton fraction was presented in Ref. 106.

5.2. *Gravitinos in R-parity Breaking Vacua*

A very well-studied candidate of decaying dark matter is the gravitino in R-parity breaking vacua (see Refs. 72,108,157,180,190–192). The gravitino, if it is the lightest supersymmetric particle (LSP), constitutes a very promising candidate for the dark matter of the Universe. The gravitino relic abundance from thermal processes is calculable using the supergravity formalism, the result being dependent on the reheating temperature of the Universe, the gravitino mass and the gluino mass.[193] It can be shown that the correct relic abundance can be achieved for gravitino and gluino masses in the 100 GeV – a few TeV range, as expected in gravity-mediated supersymmetry breaking scenarios, when the reheating temperature is around 10^{10} GeV,

which is compatible with the lower bound on the reheating temperature required by thermal leptogenesis[194] which is $T_R \gtrsim 10^9$ GeV.[195, 196] Therefore, scenarios with a gravitino in the mass range $m_{3/2} = 100$ GeV – a few TeV can accommodate both baryogenesis via leptogenesis and supersymmetric dark matter.

Despite being very attractive, this picture is not free from problems. In most analyses of supersymmetric scenarios, R-parity conservation is implicitly imposed. If this is the case, the next-to-LSP (NLSP) can only decay gravitationally into gravitinos and Standard Model particles with a lifetime such that the NLSP is present at the time of Big Bang nucleosynthesis, possibly jeopardizing the successful predictions of the standard scenario. Indeed, this is the case for most supersymmetric scenarios with gravitino dark matter. Namely, if the NLSP is a neutralino, its late decays into hadrons can dissociate the primordial elements,[197] and if the NLSP is a stau, its presence during BBN catalyzes the production of ^{6}Li, resulting in an abundance which is in conflict with observations.[198]

One simple solution to the problems induced by the NLSP in cosmology is to assume that R-parity is not exactly conserved.[191] Then, the NLSP can decay into two Standard model particles well before the onset of Big Bang nucleosynthesis, avoiding altogether the BBN constraints. When R-parity is no longer imposed, the gravitino LSP is no longer stable, but instead decays into Standard Model particles, for instance via $\psi_{3/2} \to \nu\gamma$. For the range of R-parity breaking parameters necessary to preserve the successful predictions of the standard BBN scenario and to preserve the baryon asymmetry generated by leptogenesis, the gravitino lifetime is predicted to be in the range $\tau_{3/2} = 10^{26} - 10^{40}$ s.[191] Therefore, the scenario of gravitino dark matter in R-parity breaking vacua, proposed originally to provide a consistent thermal history of the Universe with supersymmetric dark matter, thermal leptogenesis and successful Big Bang nucleosynthesis, also leads to potentially observable signatures in the cosmic-ray fluxes.[72, 83, 108, 157, 180, 192, 199–203]

In models with bilinear R-parity breaking and a non-zero sneutrino vacuum expectation value along the $\widetilde{\nu}_\tau$ direction, the main decay channels for the gravitino are:

$$
\begin{aligned}
\psi_{3/2} &\to \gamma\nu_\tau \,, \\
\psi_{3/2} &\to W^\pm\tau^\mp \,, \\
\psi_{3/2} &\to Z^0\nu_\tau \,, \\
\psi_{3/2} &\to h\nu_\tau \,.
\end{aligned}
\tag{44}
$$

The first decay is practically always allowed, while the remaining three only above the production threshold of $W^\pm$, Z^0 or h. The decay widths for these processes were calculated in Ref. 180 and the three body decays via a virtual weak gauge boson were studied in Ref. 203. The branching fractions of the different gravitino decay channels as a function of the gravitino mass are shown in Fig. 10, for a case of large Higgsino masses, gaugino masses satisfying the unification relation and giving $M_1 = 1.5\,m_{3/2}$ at the electroweak scale and $\tan\beta = 10$. As apparent from the plot, above the Z^0 mass threshold the decay channels producing weak gauge bosons in the final
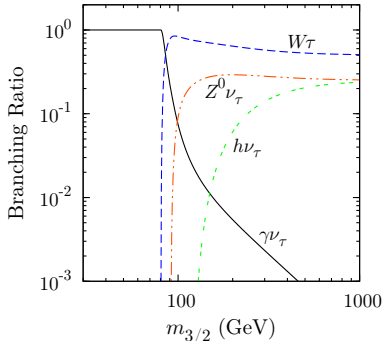
Fig. 10.   Branching ratios of the different gravitino decay channels as a function of the gravitino mass in a case of large Higgsino masses, gaugino masses satisfying the unification relation and giving $M_1 = 1.5 \, m_{3/2}$ at the electroweak scale and $\tan \beta = 10$.

state have large branching fractions, producing potentially observable signatures as an excess in the cosmic antiproton-to-proton fraction. The non-observation of an antiproton excess then allows to set a lower limit on the gravitino lifetime which is $\mathcal{O}(10^{27} - 10^{28}) \, \mathrm{s}$ for $m_{3/2} = 100 \, \mathrm{GeV} - 1 \, \mathrm{TeV}$,[108] with a strong dependence on the antiproton propagation model. Complementary limits on this scenario follow from the measurements of the gamma-ray flux by the Fermi LAT satellite, concretely from observations of the isotropic gamma-ray background and of galaxy clusters, which constrain the lifetime to be longer than $2 \times 10^{26} \, \mathrm{s}$ for $m_{3/2} = 100 \, \mathrm{GeV} - 1 \, \mathrm{TeV}$. For lower masses, the limits from searches of gamma-ray lines become fairly stringent and impose the lower limit $\tau_{3/2} \gtrsim 5 \times 10^{27} \, \mathrm{s}$ at $m_{3/2} = 100 \, \mathrm{GeV}$.[138]

5.3. *Hidden-Sector Gauginos*

Some extensions of the Minimal Supersymmetric Standard Model postulate a hidden sector containing an extra unbroken Abelian gauge symmetry. In these extensions, the hidden sector can communicate to the observable sector via the kinetic mixing term of the hidden sector Abelian vector superfield with the hypercharge vector superfield.[204–206] If the extra gauge symmetry is unbroken, the canonical normalization of the kinetic terms produces an unobservable shift of the hypercharge gauge coupling and the generation of a milli-hypercharge for the hidden sector chiral superfields. The existence of exotic particles with a milli-hypercharge is severely constrained by experiments, although the limits can be avoided when the masses of the exotic particles are large, which we assume here. Furthermore, in the limit of unbroken supersymmetry, the hypercharge vector superfield completely decouples from the observable sector and is not subject to any experimental constraint. Nevertheless, the breaking of supersymmetry dramatically changes the previous picture. Although the hidden U(1) gauge boson remains decoupled from the observable sector, in the presence of SUSY breaking effects a mixing between the hidden $U(1)$ gaugino, X, and the MSSM neutralinos, χ_i^0, is induced. In the presence of R-parity

conservation, a relic population of hidden gauginos can be generated through the mixing with the MSSM neutralinos. The production of hidden gauginos, as well as the limits on the parameters from primordial nucleosynthesis and structure formation were discussed in Ref. 207.

Depending on the masses of the hidden gaugino, M_X, and the lightest neutralino, $M_{\chi_1^0}$, one of the two particles becomes unstable with a lifetime roughly given by

$$\tau_{X,\chi_1^0} \sim \mathcal{O}(10^{-2} - 10) \times 10^{26}\,\mathrm{s} \cdot \left(\frac{M_{X,\chi_1^0}}{100\,\mathrm{GeV}} \right)^{-1} \left(\frac{\epsilon}{10^{-24}} \right)^{-2} , \tag{45}$$

where ϵ is the kinetic mixing parameter. Such small values of the kinetic mixing parameter naturally arise in specific models of compactifications of heterotic and type II strings (see e.g. Ref. 208). The decay channels are

$$\chi_1^0 \to f\bar{f}X,\, Xh^0,\, XZ^0 \quad \text{when } M_{\chi_1^0} > M_X , \tag{46}$$

$$X \to f\bar{f}\chi_i^0,\, \chi_i^0 h^0,\, \chi_i^0 Z^0,\, \chi_j^\pm W^\mp \quad \text{when } M_X > M_{\chi_1^0} , \tag{47}$$

where f denotes any lepton or quark, which branching fractions which depend on the concrete point of the MSSM parameter space. It is interesting to note that the decay is dominated by the leptonic modes in certain parameter regions of the MSSM where the sleptons are light. Thus, supersymmetric scenarios with a hidden unbroken $U(1)$ gaugino can provide a leptophilic unstable dark matter candidate. The cosmic-ray signatures of scenarios with hidden sector gauginos are discussed in Ref. 81.

5.4. *Hidden SU(2) Vectors*

Scenarios with a hidden $SU(2)$ gauge group which is spontaneously broken contain a natural dark matter candidate, the hidden vector A_μ^a, $a = 1, 2, 3$, which is long-lived due to an accidental custodial symmetry in the renormalizable Lagrangian.[209] Nevertheless, non-renormalizable dimension-six operators, suppressed by the large mass scale Λ, break the custodial symmetry and induce the decay of the dark matter particle at cosmological times, see Eq. (1). These are:

$$(\text{A}) \quad \frac{1}{\Lambda^2}\, \mathcal{D}_\mu \phi^\dagger \phi\, \mathcal{D}_\mu H^\dagger H , \tag{48}$$

$$(\text{B}) \quad \frac{1}{\Lambda^2}\, \mathcal{D}_\mu \phi^\dagger \phi\, H^\dagger \mathcal{D}_\mu H , \tag{49}$$

$$(\text{C}) \quad \frac{1}{\Lambda^2}\, \mathcal{D}_\mu \phi^\dagger \mathcal{D}_\nu \phi\, F^{\mu\nu Y} , \tag{50}$$

$$(\text{D}) \quad \frac{1}{\Lambda^2}\, \phi^\dagger F_{\mu\nu}^a \frac{\tau^a}{2} \phi F^{\mu\nu Y} , \tag{51}$$

where H the Standard Model Higgs doublet, ϕ is a complex $SU(2)_\mathrm{HS}$ doublet scalar field which breaks the symmetry, $\mathcal{D}^\mu = \partial^\mu \phi - i\frac{g_\phi}{2}\tau \cdot A^\mu$, with τ^a, $a = 1, 2, 3$ the generators of the hidden $SU(2)$ gauge group, and $F_{\mu\nu}^Y$ and $F_{\mu\nu}^a$ are the field strength tensors of the hypercharge and the hidden $SU(2)$ gauge group.
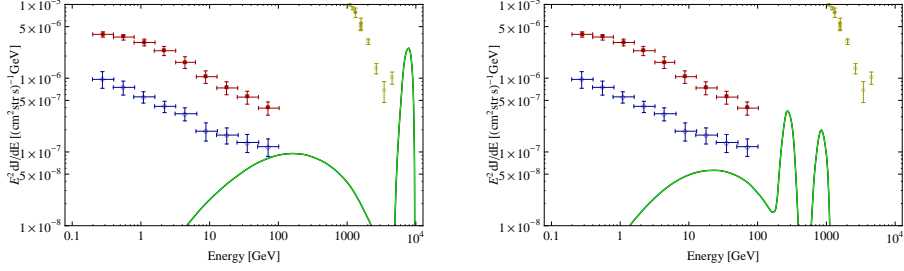
Fig. 11.   Isotropic gamma-ray signal from the decay of hidden $SU(2)$ vector dark matter particles, assuming that the decay is induced by the higher dimensional operator of the type (C), *cf.* Eq. (50). The left plot corresponds to $\tau_{\rm DM} = 6.0 \times 10^{26}$ s ($\Lambda = 2.0 \times 10^{17}$ GeV) and the right plot to $\tau_{\rm DM} = 1.6 \times 10^{27}$ s ($\Lambda = 1.2 \times 10^{16}$ GeV). From Ref. 90.

The dark matter decay modes depend on which is the dominant operator breaking the hidden sector custodial symmetry:

$$(A, B) \quad A \to \eta\eta, h\eta, hh, \gamma\eta, Z\eta, \gamma h, Zh \tag{52}$$

$$(C) \quad A \to \gamma\eta, Z\eta, \gamma h, Zh \tag{53}$$

$$(D) \quad A \to W^+W^-, Z\eta, Zh, f\bar{f}, \gamma\eta, Z\eta, \gamma h, Zh \tag{54}$$

where h and η are mass eigenstates, linear combinations of the visible and hidden sector Higgs bosons. In all cases, the decay of the hidden vector dark matter produces two gamma-ray lines, from the decays $A \to \gamma\eta$ and $A \to \gamma h$, with a rate that depends on which is the dominant operator inducing the decay. For example, in the case C, in the limit $M_\eta \ll M_A$, the inverse decay rate reads

$$\Gamma(A \to \gamma\eta)^{-1} = 2.7 \times 10^{28}\,\text{s} \left(\frac{\Lambda}{4 \times 10^{15}\,\text{GeV}}\right)^4 \left(\frac{300\,\text{GeV}}{M_A}\right)^5 , \tag{55}$$

which could be accessible to gamma-ray telescopes, depending on the scale of custodial symmetry breaking and the dark matter mass; the rate for the decay $A \to \gamma h$ is comparable. In Fig. 11 it is shown the expected isotropic gamma-ray flux in two scenarios corresponding to a decay induced by the operator of type (C). In the right plot one can clearly see the presence of two intense gamma-ray lines. It is interesting that present observations can, in this scenario, constrain the scale of the custodial symmetry to be larger than the Grand Unification Scale.

5.5. *Right-Handed Sneutrinos in Scenarios with Dirac Neutrino Masses*

A simple extension of the Minimal Supersymmetric Standard Model consists of introducing three right-handed neutrino superfields, thus allowing for neutrino oscillations. As shown in Ref. 210, 211, the right-handed sneutrinos constitute good cold dark matter candidates if R-parity is conserved and they are lighter than the

R-odd particles of the MSSM. While the R-parity conservation ensures the absolute stability of the lightest supersymmetric particle, namely the lightest right-handed sneutrino, the two heavier right-handed sneutrinos could decay into the lightest and a lepton-antilepton pair via neutralino/chargino exchange,[78] $\tilde{\nu}_{R1} \to \tilde{\nu}_{R2}\ell^+\ell^-$, $\tilde{\nu}_{R1} \to \tilde{\nu}_{R2}\nu\bar{\nu}$, provided the mass splitting between the sneutrino eigenstates is large enough to kinematically allow the decay. The decay rate for this process can then be approximated by

$$\Gamma \simeq 10^{-6} y_1^2 y_2^2 m_1 \ , \tag{56}$$

where m_1 is the mass of the decaying right-handed sneutrino and y_1 (y_2) is the Yukawa couplings of the sneutrino $\tilde{\nu}_{R1}$ ($\tilde{\nu}_{R2}$) with the neutralino/chargino and the Standard Model leptons (here it was assumed for simplicity only one generation of leptons; the generalization to three generations is straightforward). In scenarios with Dirac neutrinos the size of the Yukawa couplings is expected to be

$$y_\nu \simeq 3.0 \times 10^{-13} \left(\frac{m_\nu^2}{2.8 \times 10^{-3}\,\mathrm{eV}^2} \right)^{1/2} \ . \tag{57}$$

Using this Yukawa coupling as reference, the lifetime of the right-handed sneutrino next-to-LSP can then be cast as:

$$\tau \simeq 8 \times 10^{28}\,\mathrm{s} \left(\frac{y}{3.0 \times 10^{-13}} \right)^{-4} \left(\frac{m_{\tilde{\nu}_{R1}}}{1\,\mathrm{TeV}} \right)^{-1} \ , \tag{58}$$

which is remarkably close to the values that can be probed with cosmic ray observations.

5.6. *Hidden Gauge Bosons*

This scenario considers an extension of the Standard Model by a hidden Abelian gauge symmetry $U(1)_H$ and by a gauged $U(1)_{B-L}$ symmetry. It is further assumed that the hidden sector matter does not interact directly with either the Standard Model particles or with the $U(1)_{B-L}$; the only interaction arises through the kinetic mixing term between the $U(1)_H$ and the $U(1)_{B-L}$ (this can be arranged in an extra dimensional set-up, see Refs. 75, 212). It is also assumed that both the $U(1)_H$ and the $U(1)_{B-L}$ are spontaneously broken, such that the corresponding vector bosons acquire masses $m = \mathcal{O}(100\,\mathrm{GeV})$ and $M = \mathcal{O}(10^{15}\,\mathrm{GeV})$ respectively. Then, the relevant Lagrangian reads:

$$\mathcal{L} = -\frac{1}{4}F_{\mu\nu}^{(H)}F^{(H)\mu\nu} - \frac{1}{4}F_{\mu\nu}^{(B)}F^{(B)\mu\nu} + \frac{\lambda}{2}F_{\mu\nu}^{(H)}F^{(B)\mu\nu}$$
$$+\frac{1}{2}m^2 A_{H\mu}A_H^\mu + \frac{1}{2}M^2 A_{B\mu}A_B^\mu, \tag{59}$$

where A_H^μ and A_B^μ are the vector bosons corresponding to the $U(1)_H$ and $U(1)_{B-L}$ symmetries, while $F^{(H)\mu\nu}$ and $F^{(B)\mu\nu}$ are the corresponding field strength tensors. In the absence of a kinetic mixing term, the hidden gauge boson A^H would be completely stable. However, the kinetic mixing with the $U(1)_{B-L}$, λ, induces the

decay into the $B - L$ charged Standard Model fermions. The decay rate into a fermion-antifermion pair with $B - L$ charge q_i and color factor N_i can then be calculated to be

$$\Gamma(A_H \to \psi_i \bar{\psi}_i) \simeq \lambda^2 \frac{N_i q_i^2}{12\pi} \frac{m^5}{M^4} \ . \tag{60}$$

Hence the dark matter lifetime approximately reads:

$$\tau \ \simeq \ \frac{2.5 \times 10^{27} \sec}{\lambda^2 \sum_i N_i q_i^2} \left(\frac{m}{100 \, \text{GeV}} \right)^{-5} \left(\frac{M}{10^{15} \, \text{GeV}} \right)^4 \ . \tag{61}$$

Note that the coefficient $N_i q_i^2$ is 1/3 for quarks and 1 leptons, hence suppressing the antiproton flux.

5.7. *Neutralino Decay in R-parity Breaking Vacua*

R-parity was introduced in the Minimal Supersymmetric Standard Model to prevent too rapid proton decay. Introducing this discrete symmetry has the appealing feature that the lightest neutralino, if it is also the lightest supersymmetric particle, becomes absolutely stable and thus constitutes a perfect candidate for WIMP dark matter. However, there is no fundamental reason to assume that R-parity should be completely exact and tiny R-parity breaking parameters could leave observable signatures in cosmic rays, even for parameters yielding a proton lifetime in agreement with observations.[76, 213–215]

In the framework of the Minimal Supersymmetric Standard Model, the most general superpotential compatible with the gauge symmetry reads:

$$W = W_{MSSM} + \lambda_{ijk} L_i L_j \bar{E}_k + \lambda'_{ijk} L_i Q_j \bar{D}_k + \lambda''_{ijk} \bar{U}_i \bar{D}_j \bar{D}_k + \mu'_i L_i H_u \ , \tag{62}$$

where $i, j, k = 1, 2, 3$ are generation indices, λ, λ', λ'' are dimensionless R-parity breaking parameters and μ' has dimensions of mass. The lifetime of the lightest neutralino must then be proportional to these R-parity breaking parameters. Namely, the coupling λ'_{ijk} leads to the decays $\chi^0 \to \nu_i d_j \bar{d}_k$ and $\chi^0 \to e_i^- u_j \bar{d}_k$, while λ''_{ijk} to $\chi^0 \to u_i d_j d_k$ $(j \neq k)$. The corresponding lifetime can be estimated to be, in the limit of heavy and degenerate sfermions and assuming only a non-vanishing coupling λ',

$$\tau \sim 10^{26} \, \text{s} \times \left(\frac{\lambda'}{10^{-25}} \right)^{-2} \left(\frac{m_\chi}{1 \, \text{TeV}} \right)^{-1} \left(\frac{m_{\tilde{f}}}{m_\chi} \right)^4 \tag{63}$$

for a gaugino-like neutralino and

$$\tau \sim 10^{26} \, \text{s} \times \left(\frac{\tan \beta}{10} \right)^{-2} \left(\frac{\lambda'}{10^{-23}} \right)^{-2} \left(\frac{m_\chi}{1 \, \text{TeV}} \right)^{-1} \left(\frac{m_{\tilde{f}}}{m_\chi} \right)^4 \tag{64}$$

for a Higgsino-like neutralino. In these expressions $m_{\tilde{f}}$ is the common mass of the sfermions and $\tan \beta \equiv \langle H_u^0 \rangle / \langle H_d^0 \rangle$ is the ratio between the expectation values of the two Higgs doublets of the MSSM. The tiny R-parity violating coupling could result from higher dimensional operators suppressed by a large powers of the scale of new physics, as in certain scenarios involving flavor symmetries (see Ref. 215).

5.8. *Bound States of Strongly Interacting Particles*

The dark matter particle could be a composite state consisting of "dark quarks" from a hidden sector or from the messenger sector of supersymmetric models,[216] or techniquarks in technicolor models.[217] Quite generically, the Lagrangian contains higher- dimensional operators, suppressed by a high energy scale, which induce the dark matter decay. Therefore, the typical lifetime is given by Eq. (1) which might in principle probed in cosmic ray observations.

5.9. *Decaying Dark Matter from Dark Instantons*

The proton is the lightest baryon and therefore it is absolutely stable if the vacuum is invariant under a global $U(1)$ baryonic symmetry. This symmetry is accidental in the renormalizable part of the Lagrangian and could be broken or not by higher dimensional operators. Nevertheless, the global $U(1)$-baryonic is guaranteed to be broken by instanton $B + L$ violating effects which make the proton unstable but very long-lived, with a lifetime $\approx 10^{140}$ years.[218] This rationale was followed in Ref. 92 to construct a model where the dark matter stability is due to a global symmetry that is broken only by instanton-induced operators generated by a non-Abelian dark gauge group, $SU(2)_D \times U(1)_D$. The dark matter particle ψ is in this model predicted to decay $\psi \to \ell^+ \ell^- \nu$ with a rate

$$\Gamma \approx \frac{1}{g_D^{16}} \exp(-16\pi^2/g_D^2) \left(\frac{m_\psi}{v_D} \right)^{47/3} m_\psi \ , \qquad (65)$$

where g_D is the coupling constant and v_D the expectation value of the field that breaks the dark gauge group. Choosing $m_\psi = 3.5$ TeV, $v_D = 4$ TeV and $g_D = 1.15$ one finds a dark matter lifetime of 10^{26} s.

6. Discussion and Conclusions

While observations demonstrate that the dark matter particle is very long lived, there is no astrophysical or cosmological observation requiring its absolute stability. In fact, there are some well-motivated particle physics scenarios which predict a long-lived dark matter particle, although not absolutely stable. If the dark matter particle is indeed unstable, the decay products could be observed as an excess in the cosmic-ray fluxes of antimatter particles, gamma-rays or neutrinos over the expected backgrounds. In the last few years a myriad of new experiments have provided data of exquisite quality on the cosmic antimatter, gamma-ray and neutrino fluxes, which allow us to set independent limits on the dark matter decay width into a given final state. In this work we have focused on dark matter particles with masses in the GeV–TeV range. We have reviewed the strategies to constrain the dark matter decay width as well as the limits which follow from the most recent observations.

The non-observation of an excess in the antiproton-to-proton fraction measured by the PAMELA collaboration with respect to the expected astrophysical back-

grounds allows to set very stringent limits on the rate of decay processes containing antiprotons in the final state. Concretely, the limits on the lifetime for the decay $DM \rightarrow W^+W^-$ read $\tau_{DM} > 20(3) \times 10^{27}$ s and for the decay $DM \rightarrow b\bar{b}$, $\tau_{DM} > 15(7) \times 10^{27}$ s, in both cases for $m_{DM} = 200(2000)$ GeV and for the MED propagation model in Table 2. The positron fraction, however, shows an intriguing raise with the energy which is at the moment not understood. Dark matter decays provide a primary electron and positron flux which could account for the excess in various decay channels, if the dark matter mass is $\sim$ few TeV and the lifetime is $\sim 10^{26}$ s. Most of the models are however already in tension with the non-observation of the associated inverse Compton emission in Galaxy clusters, the isotropic gamma-ray background or the Galactic halo. No positive measurement currently exists on the cosmic antideuteron flux, thus allowing to set upper limits on the dark matter lifetime from antideuteron searches. Decay modes producing antideuterons necessarily produce antiprotons, hence there exists a strong correlation between the antiproton and the antideuteron fluxes from dark matter decay. In fact, the limits on the dark matter lifetime from the antiproton measurements are significantly stronger than the limits from antideuteron measurements, and somewhat stronger than the projected sensitivity of AMS-02 and GAPS. Therefore, the observation of antideuterons from dark matter decay in these experiments will be challenging.

Indirect signals from dark matter decay exhibit less directional dependence and amplification from regions of high dark matter density than those from traditionally considered WIMPs, since the production rate is linear in the dark matter density (as opposed to quadratic in the case of self-annihilating WIMPs). As a consequence, the strongest gamma-ray constraints on the dark matter lifetime come from observations of the extragalactic gamma-ray background, whereas observations of the Galactic center are only weakly constraining. Other important targets which yield similar sensitivity are nearby galaxy clusters. Since the extragalactic gamma-ray background is isotropic, a convincing identification of a dark matter contribution would have to mostly rely on spectral information. Fortunately, gamma-ray lines, pronounced cutoffs from final state radiation and box-shaped spectra – that are predicted in certain dark matter scenarios – could facilitate such an identification. No unambiguous dark matter signal has been found in gamma-ray observations, yet. If dark matter dominantly decays into $\bar{b}b$ or $\mu^+\mu^-$ final states, and for dark matter masses between 10 GeV – 10 TeV, Fermi LAT observations of the extragalactic gamma-ray background and the Galactic halo yield lower limits on the dark matter lifetime that range between 2×10^{25} s and 2×10^{27} s, depending on the dark matter mass. In the case of decay into $\gamma\nu$, much stronger constraints of the order 3×10^{29} s and 10^{28} s can be respectively derived from Fermi (below 300 GeV) and HESS (above 500 GeV) dedicated line searches.

Neutrino searches are challenging because of the extremely small neutrino interaction rate and the presence of large backgrounds, mainly from atmospheric neutrinos. At present, no significant excess has been observed in the diffuse neu-

Table 4. Positron Green's function coefficients from Ref. 219.

Model	a	b
M2	-0.9716	-10.012
MED	-1.0203	-1.4493
M1	-0.9809	-1.1456

trino fluxes, neither at Super-Kamiokande nor at IceCube, allowing to set the limits on the lifetime $\tau_{\mathrm{DM}} \gtrsim 10^{25}\,\mathrm{s}$ for DM $\to \nu\nu$, $\tau_{\mathrm{DM}} \gtrsim 2 \times 10^{24}\,\mathrm{s}$ for DM $\to \mu^{+}\mu^{-}$, $\tau_{\mathrm{DM}} \gtrsim 5 \times 10^{23}\,\mathrm{s}$ for DM $\to W^{+}W^{-}$ and $\tau_{\mathrm{DM}} \gtrsim 5 \times 10^{22}\,\mathrm{s}$ for DM $\to b\bar{b}$, all of them at $m_{\mathrm{DM}} = 2\,\mathrm{TeV}$.

These limits on the dark matter decay width set already stringent constraints on the parameters of models containing decaying dark matter candidates. In fact, some concrete scenarios proposed in the literature are ruled out by present observations. The main implications of the indirect searches for decaying dark matter for particle physics models are: *i)* for a scalar dark matter particle decaying into a fermion-antifermion pair, the dimensionless coupling inducing the decay must be $\lesssim \mathcal{O}(10^{-26})$ for $m_{\mathrm{DM}} = 1\,\mathrm{TeV}$, *ii)* for a spin 1/2 particle decaying into a fermion-antifermion pair and a neutrino mediated through the exchange of a heavy scalar, the couplings involved in the decay must be tiny and/or the mediator must be very heavy, concretely $M_{\Sigma} \gtrsim \mathcal{O}(10^{15}\,\mathrm{GeV})$ for $|\lambda_{\mathrm{eff}}| \sim 1$ or $|\lambda_{\mathrm{eff}}| \lesssim 10^{-12}$ for $M_{\Sigma} \sim 2\,\mathrm{TeV}$, in both cases for $m_{\mathrm{DM}} \sim 1\,\mathrm{TeV}$; similar conclusions apply when the decay is mediated by a vector, *iii)* for a spin 1/2 particle decaying into a photon and a neutrino, the effective magnetic moment must be $\lesssim \mathcal{O}(10^{-29}\,\mathrm{GeV}^{-1})$ for $m_{\mathrm{DM}} = 1\,\mathrm{TeV}$. Present indirect dark matter searches are then sensitive to physics at very high energies, close to the Grand Unification scale, or to very small couplings, possibly generated by high dimensional operators or non-perturbative effects. To conclude, we note that the interesting role of cosmic-ray measurements in probing physics at very high energies is remarkable.

Appendix A. Analytical Solutions of the Transport Equation

In this appendix we present semi-analytical solutions to the cosmic-ray transport equation, Eq. (8). Such solutions to the transport equation can be found under certain simplifying assumptions by exploiting the cylindrical geometry of the model. The first of these is that the diffusion coefficient has no spatial dependence,

Table 5. Antiproton Green's function co-
efficients for the numerical approximation,
Eq. (A.10). From Ref. 219.

Model	x	y	z
MIN	-0.0537	0.7052	-0.1840
MED	1.8002	0.4099	-0.1343
MAX	3.3602	-0.1438	-0.0403

Table 6. Antideuteron Green's function co-
efficients, from Ref. 115.

Model	x	y	z
MIN	-0.3889	0.7532	-0.1788
MED	1.6023	0.4382	-0.1270
MAX	3.1992	-0.1098	-0.0374

$K(\vec{r}, T) = K(T)$ and can be parametrized as

$$K(T) = K_0 \, \beta \, \mathcal{R}^\delta \, . \tag{A.1}$$

For positrons and electrons we can neglect diffusive reacceleration, annihila-
tion in the Galactic disk and convection. We further assume the simplified form
of the electron energy loss rate, $b(E) = \frac{1}{\tau_E} \left(\frac{E}{E_0} \right)^2$. As a result, we can describe
electron/positron propagation in terms of only three parameters which have to be
determined from observation, namely δ, K_0 and L. We list three sets of parameters
in Table 2. If we make the aforementioned simplifications of spatially constant diffu-
sion and energy loss rates, the transport equation can be solved semi-analytically as
a series in Bessel and sin functions. The solution for the Green's function is:[220, 221]

$$G_{e^+}(T, T') = \sum_{n,m=1}^\infty B_{nm}(T, T') J_0 \left(\zeta_n \frac{r_\odot}{R} \right) \sin \left(\frac{m\pi}{2} \right) \, , \tag{A.2}$$

where the coefficients are given by

$$B_{nm}(T, T') = \frac{\tau_E T_0}{T^2} C_{nm} \times$$
$$\times \exp \left\{ \left(\frac{\zeta_n^2}{R^2} + \frac{m^2 \pi^2}{4L^2} \right) \frac{K_0 \tau_E}{\delta - 1} \left[\left(\frac{T}{T_0} \right)^{\delta-1} - \left(\frac{T'}{T_0} \right)^{\delta-1} \right] \right\} \, , \tag{A.3}$$

with

$$C_{nm} = \frac{2}{J_1^2(\zeta_n) R^2 L} \int_0^R dr' \, r' \int_{-L}^L dz' \, \rho_{\mathrm{DM}}(\vec{r}') J_0 \left(\zeta_n \frac{r'}{R} \right) \sin \left[\frac{m\pi}{2L}(L - z') \right] \, . \tag{A.4}$$

For simplicity one can approximate the above Green's function numerically by
a rather simple parametrization instead of computing the full solution above. The

following simple function yields good numerical agreement with the semi-analytical solution:[219]

$$G_{e^+}(T,T') \simeq \frac{10^{16}}{T^2} e^{a+b(T^{\delta-1}-T'^{\delta-1})} \theta(T'-T) \text{ cm}^{-3} \text{ s}. \tag{A.5}$$

We list the coefficients a and b in Table 4 for the NFW dark matter profile and the MIN, MED and MAX sets of transport parameters.

For antiprotons and antideuterons we can neglect energy losses. We further assume that the convective wind has axial direction away from the Galactic disk. The analytic solution for the Green's function then reads

$$G_{\bar{p}}(T,T') = \sum_{i=1}^{\infty} \exp\left(-\frac{V_c L}{2K(T)}\right) \frac{y_i(T)}{A_i(T)\sinh(S_i(T)L/2)} J_0\left(\zeta_i \frac{r_\odot}{R}\right) \delta(T-T') \tag{A.6}$$

where

$$y_i(T) = \frac{4}{J_1^2(\zeta_i)R^2} \int_0^R dr'\, r' J_0\left(\zeta_i \frac{r'}{R}\right) \int_0^L dz'\, \exp\left(\frac{V_c(L-z')}{2K(T)}\right) \times$$
$$\times \sinh\left(\frac{S_i(L-z')}{2}\right) \rho_{\text{DM}}(\vec{r}') \tag{A.7}$$

and

$$A_i(T) = 2h\Gamma_{\text{ann}} + V_c + kS_i(T)\coth\left(\frac{S_i(T)L}{2}\right), \tag{A.8}$$

$$S_i(T) = \sqrt{\frac{V_c^2}{K(T)^2} + \frac{4\zeta_i^2}{R^2}}. \tag{A.9}$$

The Green's function for antiproton propagation can be approximated numerically by the following simple function:[219]

$$G_{\bar{p}}(T,T') \simeq 10^{14} e^{x+y\ln T+z\ln^2 T} \delta(T'-T) \text{ cm}^{-3} \text{ s}, \tag{A.10}$$

where the coefficients x, y and z are given in Table 5 for the NFW dark matter profile and the MIN, MED and MAX set of propagation parameters. The approximation is better than 10% compared to the full analytical solution. As mentioned before, the choice of halo profile does not substantially affect the resulting cosmic-ray fluxes in the case of decaying dark matter. The case of antideuteron propagation is almost identical to antiproton propagation and can be approximated using the same parametrization, Eq. (A.10). The corresponding parameters for the case of antideuterons are shown in Table 6.

References

1. G. Bertone, D. Hooper and J. Silk, *Phys.Rept.* **405**, 279 (2005), arXiv:hep-ph/0404175 [hep-ph].
2. L. Bergstrom, *Annalen Phys.* **524**, 479 (2012), arXiv:1205.4882 [astro-ph.HE].
3. G. Jungman, M. Kamionkowski and K. Griest, *Phys.Rept.* **267**, 195 (1996), arXiv:hep-ph/9506380 [hep-ph].

4. Super-Kamiokande Collaboration Collaboration (H. Nishino *et al.*), *Phys.Rev.Lett.* **102**, 141801 (2009), `arXiv:0903.0676 [hep-ex]`.
5. H. Back, M. Balata, A. de Bari, T. Beau, A. de Bellefon *et al.*, *Phys.Lett.* **B525**, 29 (2002).
6. A. Mirizzi, D. Montanino and P. D. Serpico, *Phys.Rev.* **D76**, 053007 (2007), `arXiv:0705.4667 [hep-ph]`.
7. Particle Data Group Collaboration (J. Beringer *et al.*), *Phys.Rev.* **D86**, 010001 (2012).
8. D. Eichler, *Phys. Rev. Lett.* **63**, 2440 (1989).
9. Planck Collaboration Collaboration (P. Ade *et al.*) (2013), `arXiv:1303.5076 [astro-ph.CO]`.
10. J. F. Navarro, C. S. Frenk and S. D. M. White, *Astrophys. J.* **462**, 563 (1996), `arXiv:astro-ph/9508025`.
11. J. F. Navarro, C. S. Frenk and S. D. M. White, *Astrophys. J.* **490**, 493 (1997), `arXiv:astro-ph/9611107 [astro-ph]`.
12. M. Cirelli *et al.*, *JCAP* **1103**, 051 (2011), `arXiv:1012.4515 [hep-ph]`.
13. J. F. Navarro, E. Hayashi, C. Power, A. Jenkins, C. S. Frenk *et al.*, *Mon.Not.Roy.Astron.Soc.* **349**, 1039 (2004), `arXiv:astro-ph/0311231 [astro-ph]`.
14. A. W. Graham, D. Merritt, B. Moore, J. Diemand and B. Terzic, *Astron.J.* **132**, 2685 (2006), `arXiv:astro-ph/0509417 [astro-ph]`.
15. J. F. Navarro, A. Ludlow, V. Springel, J. Wang, M. Vogelsberger *et al.* (2008), `arXiv:0810.1522 [astro-ph]`.
16. J. N. Bahcall and R. Soneira, *Astrophys.J.Suppl.* **44**, 73 (1980).
17. R. Catena and P. Ullio, *JCAP* **1008**, 004 (2010), `arXiv:0907.0018 [astro-ph.CO]`.
18. M. Weber and W. de Boer, *Astron.Astrophys.* **509**, A25 (2010), `arXiv:0910.4272 [astro-ph.CO]`.
19. P. Salucci, F. Nesti, G. Gentile and C. Martins, *Astron.Astrophys.* **523**, A83 (2010), `arXiv:1003.3101 [astro-ph.GA]`.
20. M. Pato, O. Agertz, G. Bertone, B. Moore and R. Teyssier, *Phys.Rev.* **D82**, 023531 (2010), `arXiv:1006.1322 [astro-ph.HE]`.
21. F. Iocco, M. Pato, G. Bertone and P. Jetzer, *JCAP* **1111**, 029 (2011), `arXiv:1107.5810 [astro-ph.GA]`.
22. A. Boyarsky, O. Ruchayskiy and M. Shaposhnikov, *Ann. Rev. Nucl. Part. Sci.* **59**, 191 (2009), `arXiv:0901.0011 [hep-ph]`.
23. A. Merle, *Int.J.Mod.Phys.* **D22**, 1330020 (2013), `arXiv:1302.2625 [hep-ph]`.
24. M. Cirelli, *Pramana* **79**, 1021 (2012), `arXiv:1202.1454 [hep-ph]`.
25. T. Bringmann and C. Weniger, *Phys.Dark Univ.* **1**, 194 (2012), `arXiv:1208.5481 [hep-ph]`.
26. V. S. Berezinskii, S. V. Buolanov, V. A. Dogiel, V. L. Ginzburg, V. S. Ptuskin, *Astrophysics of Cosmic Rays* (North-Holland, 1990).
27. A. W. Strong, I. V. Moskalenko and V. S. Ptuskin, *Ann.Rev.Nucl.Part.Sci.* **57**, 285 (2007), `arXiv:astro-ph/0701517 [astro-ph]`.
28. D. Maurin, F. Donato, R. Taillet and P. Salati, *Astrophys. J.* **555**, 585 (2001), `arXiv:astro-ph/0101231`.
29. T. Bringmann, F. Donato and R. A. Lineros, *JCAP* **1201**, 049 (June 2012), `1106.4821`.
30. G. Di Bernardo, C. Evoli, D. Gaggero, D. Grasso and L. Maccione, *JCAP* **1303**, 036 (2013), `arXiv:1210.4546 [astro-ph.HE]`.
31. `http://galprop.stanford.edu/`.
32. `http://www.desy.de/~maccione/DRAGON/index.html`.

33. L. J. Gleeson and W. I. Axford, *Astrophys.J.* **149**, L115 (1967).
34. L. J. Gleeson and W. I. Axford, *Astrophys.J.* **154**, 1011 (1968).
35. J. S. Perko, *Astron. Astrophys.* **184**, 119 (1987).
36. T. Delahaye *et al.*, *Astron. Astrophys.* **501**, 821 (2009), `arXiv:0809.5268 [astro-ph]`.
37. P. Salati, *PoS* **CARGESE2007**, 009 (2007).
38. T. A. Porter and A. Strong (2005), `arXiv:astro-ph/0507119`.
39. A. W. Strong, I. V. Moskalenko and O. Reimer, *Astrophys. J.* **537**, 763 (2000), `arXiv:astro-ph/9811296`.
40. K. Ishiwata, S. Matsumoto and T. Moroi, *Phys. Rev.* **D79**, 043527 (2009), `arXiv:0811.4492 [astro-ph]`.
41. L. Zhang, G. Sigl and J. Redondo, *JCAP* **0909**, 012 (2009), `arXiv:0905.4952 [astro-ph.GA]`.
42. L. Zhang, C. Weniger, L. Maccione, J. Redondo and G. Sigl, *JCAP* **1006**, 027 (2010), `arXiv:0912.4504 [astro-ph.HE]`.
43. I. V. Moskalenko and A. W. Strong, *Astrophys. J.* **493**, 694 (1998), `arXiv:astro-ph/9710124`.
44. AMS-01 Collaboration (M. Aguilar *et al.*), *Phys. Lett.* **B646**, 145 (2007), `arXiv:astro-ph/0703154`.
45. HEAT Collaboration Collaboration (S. Barwick *et al.*), *Astrophys.J.* **482**, L191 (1997), `arXiv:astro-ph/9703192 [astro-ph]`.
46. J. Beatty, A. Bhattacharyya, C. Bower, S. Coutu, M. DuVernois *et al.*, *Phys.Rev.Lett.* **93**, 241102 (2004), `arXiv:astro-ph/0412230 [astro-ph]`.
47. CAPRICE Collaboration Collaboration (M. Boezio *et al.*), *Astrophys.J.* **532**, 653 (2000).
48. PAMELA Collaboration (O. Adriani *et al.*), *Nature* **458**, 607 (2009), `arXiv:0810.4995 [astro-ph]`.
49. AMS Collaboration Collaboration (M. Aguilar *et al.*), *Phys.Rev.Lett.* **110**, 141102 (2013).
50. P. D. Serpico, *Phys.Rev.* **D79**, 021302 (2009), `arXiv:0810.4846 [hep-ph]`.
51. O. Adriani, G. Barbarino, G. Bazilevskaya, R. Bellotti, M. Boezio *et al.*, *Astropart.Phys.* **34**, 1 (2010), `arXiv:1001.3522 [astro-ph.HE]`.
52. The Fermi LAT Collaboration (M. Ackermann *et al.*), *Phys.Rev.Lett.* **108**, 011103 (2012), `arXiv:1109.0521 [astro-ph.HE]`.
53. Fermi LAT Collaboration (A. A. Abdo *et al.*), *Phys. Rev. Lett.* **102**, 181101 (2009), `arXiv:0905.0025 [astro-ph.HE]`.
54. J. Chang, J. Adams, H. Ahn, G. Bashindzhagyan, M. Christl *et al.*, *Nature* **456**, 362 (2008).
55. PPB-BETS Collaboration Collaboration (S. Torii *et al.*) (2008), `arXiv:0809.0760 [astro-ph]`.
56. H.E.S.S. Collaboration Collaboration (F. Aharonian *et al.*), *Phys.Rev.Lett.* **101**, 261104 (2008), `arXiv:0811.3894 [astro-ph]`.
57. H.E.S.S. Collaboration (F. Aharonian *et al.*), *Astron. & Astrophys.* **508**, 561 (2009), `arXiv:0905.0105 [astro-ph.HE]`.
58. Fermi LAT Collaboration (D. Grasso *et al.*), *Astropart. Phys.* **32**, 140 (2009), `arXiv:0905.0636 [astro-ph.HE]`.
59. A. Ibarra, D. Tran and C. Weniger, *JCAP* **1001**, 009 (2010), `arXiv:0906.1571 [hep-ph]`.
60. H. Gast and S. Schael, *Proceedings of the 31st International Cosmic Ray Conference* (2009).

61. A. M. Atoian, F. A. Aharonian and H. J. Volk, *Phys. Rev.* **D52**, 3265 (1995).
62. D. Hooper, P. Blasi and P. D. Serpico, *JCAP* **0901**, 025 (2009), `arXiv:0810.1527 [astro-ph]`.
63. C. Grimani, *Astron. Astrophys.* **418**, 649 (2004).
64. K. Ioka, *Prog.Theor.Phys.* **123**, 743 (2010), `arXiv:0812.4851 [astro-ph]`.
65. N. J. Shaviv, E. Nakar and T. Piran, *Phys.Rev.Lett.* **103**, 111302 (2009), `arXiv:0902.0376 [astro-ph.HE]`.
66. P. Blasi and P. D. Serpico, *Phys.Rev.Lett.* **103**, 081103 (2009), `arXiv:0904.0871 [astro-ph.HE]`.
67. M. Ahlers, P. Mertsch and S. Sarkar, *Phys.Rev.* **D80**, 123017 (2009), `arXiv:0909.4060 [astro-ph.HE]`.
68. Y. Fujita, K. Kohri, R. Yamazaki, K. Ioka, K. Kohri *et al.*, *Phys.Rev.* **D80**, 063003 (2009), `arXiv:0903.5298 [astro-ph.HE]`.
69. A. Ibarra and D. Tran, *JCAP* **0902**, 021 (2009), `arXiv:0811.1555 [hep-ph]`.
70. C.-R. Chen, F. Takahashi and T. T. Yanagida, *Phys. Lett.* **B671**, 71 (2009), `arXiv:0809.0792 [hep-ph]`.
71. A. Arvanitaki *et al.*, *Phys. Rev.* **D79**, 105022 (2009), `arXiv:0812.2075 [hep-ph]`.
72. K. Ishiwata, S. Matsumoto and T. Moroi, *Phys.Rev.* **D78**, 063505 (2008), `arXiv:0805.1133 [hep-ph]`.
73. K. Ishiwata, S. Matsumoto and T. Moroi, *Phys. Lett.* **B675**, 446 (2009), `arXiv:0811.0250 [hep-ph]`.
74. C.-R. Chen and F. Takahashi, *JCAP* **0902**, 004 (2009), `arXiv:0810.4110 [hep-ph]`.
75. C.-R. Chen, M. M. Nojiri, F. Takahashi and T. T. Yanagida, *Prog. Theor. Phys.* **122**, 553 (2009), `arXiv:0811.3357 [astro-ph]`.
76. P.-f. Yin, Q. Yuan, J. Liu, J. Zhang, X.-j. Bi *et al.*, *Phys.Rev.* **D79**, 023512 (2009), `arXiv:0811.0176 [hep-ph]`.
77. K. Hamaguchi, S. Shirai and T. T. Yanagida, *Phys. Lett.* **B673**, 247 (2009), `arXiv:0812.2374 [hep-ph]`.
78. M. Pospelov and M. Trott, *JHEP* **04**, 044 (2009), `arXiv:0812.0432 [hep-ph]`.
79. A. Arvanitaki *et al.*, *Phys. Rev.* **D80**, 055011 (2009), `arXiv:0904.2789 [hep-ph]`.
80. K. J. Bae and B. Kyae, *JHEP* **05**, 102 (2009), `arXiv:0902.3578 [hep-ph]`.
81. A. Ibarra, A. Ringwald, D. Tran and C. Weniger, *JCAP* **0908**, 017 (2009), `arXiv:0903.3625 [hep-ph]`.
82. K. Cheung, P.-Y. Tseng and T.-C. Yuan, *Phys. Lett.* **B678**, 293 (2009), `arXiv:0902.4035 [hep-ph]`.
83. S.-L. Chen, R. N. Mohapatra, S. Nussinov and Y. Zhang, *Phys.Lett.* **B677**, 311 (2009), `arXiv:0903.2562 [hep-ph]`.
84. J. Hisano, K. Nakayama and M. J. S. Yang, *Phys. Lett.* **B678**, 101 (2009), `arXiv:0905.2075 [hep-ph]`.
85. H. Fukuoka, J. Kubo and D. Suematsu, *Phys. Lett.* **B678**, 401 (2009), `arXiv:0905.2847 [hep-ph]`.
86. S. Shirai, F. Takahashi and T. T. Yanagida, *Phys. Lett.* **B675**, 73 (2009), `arXiv:0902.4770 [hep-ph]`.
87. K.-Y. Choi, D. E. Lopez-Fogliani, C. Munoz and R. R. de Austri, *JCAP* **1003**, 028 (2010), `arXiv:0906.3681 [hep-ph]`.
88. K. Kohri, A. Mazumdar, N. Sahu and P. Stephens, *Phys. Rev.* **D80**, 061302 (2009), `arXiv:0907.0622 [hep-ph]`.
89. J. Mardon, Y. Nomura and J. Thaler, *Phys.Rev.* **D80**, 035013 (2009), `arXiv:0905.3749 [hep-ph]`.
90. C. Arina, T. Hambye, A. Ibarra and C. Weniger, *JCAP* **1003**, 024 (2010),

arXiv:0912.4496 [hep-ph].

91. N. F. Bell, A. J. Galea and K. Petraki, *Phys.Rev.* **D82**, 023514 (2010), arXiv:1004.1008 [astro-ph.HE].

92. C. D. Carone, J. Erlich and R. Primulando, *Phys.Rev.* **D82**, 055028 (2010), arXiv:1008.0642 [hep-ph].

93. M. Ibe, S. Matsumoto, S. Shirai and T. T. Yanagida, *JHEP* **1307**, 063 (2013), arXiv:1305.0084 [hep-ph].

94. K. R. Dienes, J. Kumar and B. Thomas (2013), arXiv:1306.2959 [hep-ph].

95. H.-B. Jin, Y.-L. Wu and Y.-F. Zhou (2013), arXiv:1304.1997 [hep-ph].

96. L. Bergstrom, T. Bringmann, I. Cholis, D. Hooper and C. Weniger, *Phys.Rev.Lett.* (2013), arXiv:1306.3983 [astro-ph.HE].

97. A. Ibarra, A. S. Lamperstorfer and J. Silk (2013), arXiv:1309.2570 [hep-ph].

98. L. Feng and Z. Kang (2013), arXiv:1304.7492 [hep-ph].

99. I. Masina and F. Sannino, *JCAP* **1109**, 021 (2011), arXiv:1106.3353 [hep-ph].

100. PAMELA Collaboration Collaboration (O. Adriani *et al.*), *Phys.Rev.Lett.* **105**, 121101 (2010), arXiv:1007.0821 [astro-ph.HE].

101. O. Adriani, G. Bazilevskaya, G. Barbarino, R. Bellotti, M. Boezio *et al.*, *JETP Lett.* **96**, 621 (2013).

102. L. Bergström, J. Edsjö and P. Ullio, *Astrophys. J.* **526**, 215 (1999), arXiv:astro-ph/9902012.

103. F. Donato, D. Maurin, P. Salati, A. Barrau, G. Boudoul *et al.*, *Astrophys.J.* **563**, 172 (2001), arXiv:astro-ph/0103150 [astro-ph].

104. L. Tan and L. Ng, *J.Phys.* **G9**, 227 (1983).

105. R. Protheroe, *Astrophys.J.* **251**, 387 (1981).

106. M. Garny, A. Ibarra and D. Tran, *JCAP* **1208**, 025 (2012), arXiv:1205.6783 [hep-ph].

107. I. Cholis, *JCAP* **1109**, 007 (2011), arXiv:1007.1160 [astro-ph.HE].

108. T. Delahaye and M. Grefe (2013), arXiv:1305.7183 [hep-ph].

109. H. Fuke, T. Maeno, K. Abe, S. Haino, Y. Makida *et al.*, *Phys.Rev.Lett.* **95**, 081101 (2005), arXiv:astro-ph/0504361 [astro-ph].

110. P. von Doetinchem (2012), talk at the 9th International Conference *Identification of Dark Matter*, July 23-27 2012, Chicago, USA.

111. R. Duperray, B. Baret, D. Maurin, G. Boudoul, A. Barrau *et al.*, *Phys.Rev.* **D71**, 083013 (2005), arXiv:astro-ph/0503544 [astro-ph].

112. F. Donato, N. Fornengo and D. Maurin, *Phys.Rev.* **D78**, 043506 (2008), arXiv:0803.2640 [hep-ph].

113. F. Donato, N. Fornengo and P. Salati, *Phys.Rev.* **D62**, 043003 (2000), arXiv:hep-ph/9904481 [hep-ph].

114. A. Ibarra and S. Wild (2013), arXiv:1301.3820 [astro-ph.HE].

115. A. Ibarra and D. Tran, *JCAP* **0906**, 004 (2009), arXiv:0904.1410 [hep-ph].

116. A. Ibarra and S. Wild, *JCAP* **1302**, 021 (2013), arXiv:1209.5539 [hep-ph].

117. S. Butler and C. Pearson, *Phys.Rev.* **129**, 836 (1963).

118. A. Schwarzschild and C. Zupancic, *Phys.Rev.* **129**, 854 (1963).

119. L. Csernai and J. I. Kapusta, *Phys.Rept.* **131**, 223 (1986).

120. M. Kadastik, M. Raidal and A. Strumia, *Phys. Lett.* **B683**, 248 (2010), arXiv:0908.1578 [hep-ph].

121. ALEPH Collaboration Collaboration (S. Schael *et al.*), *Phys.Lett.* **B639**, 192 (2006), arXiv:hep-ex/0604023 [hep-ex].

122. N. Fornengo, L. Maccione and A. Vittino (2013), arXiv:1306.4171 [hep-ph].

123. G. Bertone, W. Buchmüller, L. Covi and A. Ibarra, *JCAP* **0711**, 003 (2007),

arXiv:0709.2299 [astro-ph].

124. A. Ibarra, D. Tran and C. Weniger, *Phys. Rev.* **D81**, 023529 (2010), arXiv:0909.3514 [hep-ph].
125. A. Dominguez, J. Primack, D. Rosario, F. Prada, R. Gilmore *et al.* (2010), arXiv:1007.1459 [astro-ph.CO].
126. MAGIC Collaboration Collaboration (E. Aliu *et al.*), *Science* **320**, 1752 (2008), arXiv:0807.2822 [astro-ph].
127. GBM Collaboration Collaboration (A. Abdo *et al.*), *Astrophys.J.* **723**, 1082 (2010), arXiv:1005.0996 [astro-ph.HE].
128. A. Cuesta, T. Jeltema, F. Zandanel, S. Profumo, F. Prada *et al.*, *Astrophys.J.* **726**, L6 (2011), arXiv:1007.3469 [astro-ph.HE].
129. L. Dugger, T. E. Jeltema and S. Profumo, *JCAP* **1012**, 015 (2010), arXiv:1009.5988 [astro-ph.HE].
130. G. R. Blumenthal and R. J. Gould, *Rev. Mod. Phys.* **42**, 237 (1970).
131. K. Ishiwata, S. Matsumoto and T. Moroi, *Phys. Lett.* **B679**, 1 (2009), arXiv:0905.4593 [astro-ph.CO].
132. C. Boehm, T. Delahaye and J. Silk, *Phys. Rev. Lett.* **105**, 221301 (2010), arXiv:1003.1225 [astro-ph.GA].
133. Fermi LAT Collaboration (A. A. Abdo *et al.*), *Phys. Rev. Lett.* **104**, 101101 (2010), arXiv:1002.3603 [astro-ph.HE].
134. M. Ackermann (2012), Talk at Fermi Symposium, 29 Oct–2 Nov 2012, Monterey, USA.
135. M. Cirelli, E. Moulin, P. Panci, P. D. Serpico and A. Viana, *Phys.Rev.* **D86**, 083506 (2012), arXiv:1205.5283 [astro-ph.CO].
136. M. Ackermann (2011), Talk at TeVPA, 1–5 Aug 2011, Stockholm, Sweden.
137. T. Bringmann, F. Calore, M. Di Mauro and F. Donato (2013), arXiv:1303.3284 [astro-ph.CO].
138. X. Huang, G. Vertongen and C. Weniger, *JCAP* **1201**, 042 (2012), arXiv:1110.1529 [hep-ph].
139. LAT collaboration Collaboration (M. Ackermann *et al.*), *Astrophys.J.* **761**, 91 (2012), arXiv:1205.6474 [astro-ph.CO].
140. Fermi-LAT Collaboration Collaboration (M. Ackermann *et al.*) (2013), arXiv:1305.5597 [astro-ph.HE].
141. H.E.S.S. Collaboration Collaboration (A. Abramowski *et al.*), *Phys.Rev.Lett.* **110**, 041301 (2013), arXiv:1301.1173 [astro-ph.HE].
142. C.-R. Chen, S. K. Mandal and F. Takahashi, *JCAP* **1001**, 023 (2010), arXiv:0910.2639 [hep-ph].
143. M. Cirelli, P. Panci and P. D. Serpico, *Nucl. Phys.* **B840**, 284 (2010), arXiv:0912.0663 [astro-ph.CO].
144. M. Papucci and A. Strumia, *JCAP* **1003**, 014 (2010), arXiv:0912.0742 [hep-ph].
145. K. Ishiwata, S. Matsumoto and T. Moroi, *JHEP* **1012**, 006 (2010), arXiv:1008.3636 [hep-ph].
146. G. Hutsi, A. Hektor and M. Raidal, *JCAP* **1007**, 008 (2010), arXiv:1004.2036 [astro-ph.HE].
147. F. Calore, V. De Romeri and F. Donato, *Phys.Rev.* **D85**, 023004 (2012), arXiv:1105.4230 [astro-ph.CO].
148. Fermi LAT Collaboration (A. A. Abdo *et al.*), *JCAP* **1004**, 014 (2010), arXiv:1002.4415 [astro-ph.CO].
149. G. Dobler, D. P. Finkbeiner, I. Cholis, T. R. Slatyer and N. Weiner, *Astrophys. J.* **717**, 825 (2010), arXiv:0910.4583 [astro-ph.HE].

150. M. Su, T. R. Slatyer and D. P. Finkbeiner, *Astrophys. J.* **724**, 1044 (2010), `arXiv:1005.5480 [astro-ph.HE]`.
151. M. Garny, A. Ibarra, D. Tran and C. Weniger, *JCAP* **1101**, 032 (2011), `arXiv:1011.3786 [hep-ph]`.
152. J. Ke, M. Luo, L. Wang and G. Zhu, *Phys. Lett.* **B698**, 44 (2011), `arXiv:1101.5878 [hep-ph]`.
153. M. Luo, L. Wang and G. Zhu, *Mod.Phys.Lett.* **A27**, 1250206 (2012), `arXiv:1107.3024 [hep-ph]`.
154. C. Combet, D. Maurin, E. Nezri, E. Pointecouteau, J. Hinton *et al.*, *Phys.Rev.* **D85**, 063517 (2012), `arXiv:1203.1164 [astro-ph.CO]`.
155. R. Essig, N. Sehgal and L. E. Strigari, *Phys. Rev.* **D80**, 023506 (2009), `arXiv:0902.4750 [hep-ph]`.
156. S. Palomares-Ruiz and J. M. Siegal-Gaskins, *JCAP* **1007**, 023 (2010), `arXiv:1003.1142 [astro-ph.CO]`.
157. A. Ibarra and D. Tran, *Phys. Rev. Lett.* **100**, 061301 (2008), `arXiv:0709.4593 [astro-ph]`.
158. A. Ibarra, S. Lopez Gehler and M. Pato, *JCAP* **1207**, 043 (2012), `arXiv:1205.0007 [hep-ph]`.
159. A. Abdo, M. Ackermann, M. Ajello, W. Atwood, L. Baldini *et al.*, *Phys.Rev.Lett.* **104**, 091302 (2010), `arXiv:1001.4836 [astro-ph.HE]`.
160. G. Vertongen and C. Weniger, *JCAP* **1105**, 027 (2011), `arXiv:1101.2610 [hep-ph]`.
161. T. Bringmann, X. Huang, A. Ibarra, S. Vogl and C. Weniger, *JCAP* **1207**, 054 (2012), `arXiv:1203.1312 [hep-ph]`.
162. C. Weniger, *JCAP* **1208**, 007 (2012), `arXiv:1204.2797 [hep-ph]`.
163. LAT Collaboration Collaboration (M. Ackermann *et al.*), *Phys.Rev.* **D86**, 022002 (2012), `arXiv:1205.2739 [astro-ph.HE]`.
164. E. Tempel, A. Hektor and M. Raidal, *JCAP* **1209**, 032 (2012), `arXiv:1205.1045 [hep-ph]`.
165. M. Su and D. P. Finkbeiner (2012), `arXiv:1206.1616 [astro-ph.HE]`.
166. W. Buchmuller and M. Garny, *JCAP* **1208**, 035 (2012), `arXiv:1206.7056 [hep-ph]`.
167. B. Kyae and J.-C. Park, *Phys.Lett.* **B718**, 1425 (2013), `arXiv:1205.4151 [hep-ph]`.
168. L. Bergstrom, G. Bertone, J. Conrad, C. Farnier and C. Weniger, *JCAP* **1211**, 025 (2012), `arXiv:1207.6773 [hep-ph]`.
169. M. Gonzalez-Garcia, M. Maltoni, J. Salvado and T. Schwetz, *JHEP* **1212**, 123 (2012), `arXiv:1209.3023 [hep-ph]`.
170. M. Honda, T. Kajita, K. Kasahara, S. Midorikawa and T. Sanuki, *Phys.Rev.* **D75**, 043006 (2007), `arXiv:astro-ph/0611418 [astro-ph]`.
171. L. Pasquali and M. Reno, *Phys.Rev.* **D59**, 093003 (1999), `arXiv:hep-ph/9811268 [hep-ph]`.
172. G. Ingelman and M. Thunman, *Phys.Rev.* **D54**, 4385 (1996), `arXiv:hep-ph/9604288 [hep-ph]`.
173. H. Athar, F.-F. Lee and G.-L. Lin, *Phys. Rev. D* **71**, 103008 (2005), `arXiv:hep-ph/0407183`.
174. Frejus Collaboration. Collaboration (K. Daum *et al.*), *Z.Phys.* **C66**, 417 (1995).
175. M. Gonzalez-Garcia, M. Maltoni and J. Rojo, *JHEP* **0610**, 075 (2006), `arXiv:hep-ph/0607324 [hep-ph]`.
176. IceCube Collaboration Collaboration (R. Abbasi *et al.*), *Phys.Rev.* **D79**, 102005 (2009), `arXiv:0902.0675 [astro-ph.HE]`.
177. D. Chirkin (2009), Talk at the 31st ICRC conference, 7-15 July 2009, Lodz, Poland.
178. IceCube Collaboration Collaboration (R. Abbasi *et al.*), *Phys.Rev.* **D84**, 082001

(2011), arXiv:1104.5187 [astro-ph.HE].

179. L. Covi, M. Grefe, A. Ibarra and D. Tran, *JCAP* **1004**, 017 (2010), arXiv:0912.3521 [hep-ph].
180. L. Covi, M. Grefe, A. Ibarra and D. Tran, *JCAP* **0901**, 029 (2009), arXiv:0809.5030 [hep-ph].
181. J. Hisano, M. Kawasaki, K. Kohri and K. Nakayama, *Phys.Rev.* **D79**, 043516 (2009), arXiv:0812.0219 [hep-ph].
182. S. Palomares-Ruiz, *Phys.Lett.* **B665**, 50 (2008), arXiv:0712.1937 [astro-ph].
183. F.-F. Lee and G.-L. Lin, *Phys.Rev.* **D85**, 023529 (2012), arXiv:1105.5719 [hep-ph].
184. IceCube Collaboration Collaboration (R. Abbasi *et al.*), *Phys.Rev.* **D84**, 022004 (2011), arXiv:1101.3349 [astro-ph.HE].
185. A. Esmaili, A. Ibarra and O. L. Peres, *JCAP* **1211**, 034 (2012), arXiv:1205.5281 [hep-ph].
186. K. Murase and J. F. Beacom, *JCAP* **1210**, 043 (2012), arXiv:1206.2595 [hep-ph].
187. M. Gustafsson, T. Hambye and T. Scarna, *Phys.Lett.* **B724**, 288 (2013), arXiv:1303.4423 [hep-ph].
188. C. Giunti and A. Studenikin, *Phys.Atom.Nucl.* **72**, 2089 (2009), arXiv:0812.3646 [hep-ph].
189. CTA Consortium Collaboration (M. Actis *et al.*), *Exper.Astron.* **32**, 193 (2011), arXiv:1008.3703 [astro-ph.IM].
190. F. Takayama and M. Yamaguchi, *Phys.Lett.* **B485**, 388 (2000), arXiv:hep-ph/0005214 [hep-ph].
191. W. Buchmuller, L. Covi, K. Hamaguchi, A. Ibarra and T. Yanagida, *JHEP* **0703**, 037 (2007), arXiv:hep-ph/0702184 [HEP-PH].
192. K. Ishiwata, S. Matsumoto and T. Moroi, *JHEP* **0905**, 110 (2009), arXiv:0903.0242 [hep-ph].
193. M. Bolz, A. Brandenburg and W. Buchmuller, *Nucl.Phys.* **B606**, 518 (2001), arXiv:hep-ph/0012052 [hep-ph].
194. M. Fukugita and T. Yanagida, *Phys.Lett.* **B174**, 45 (1986).
195. S. Davidson and A. Ibarra, *Phys.Lett.* **B535**, 25 (2002), arXiv:hep-ph/0202239 [hep-ph].
196. W. Buchmuller, P. Di Bari and M. Plumacher, *Annals Phys.* **315**, 305 (2005), arXiv:hep-ph/0401240 [hep-ph].
197. M. Kawasaki, K. Kohri and T. Moroi, *Phys.Rev.* **D71**, 083502 (2005), arXiv:astro-ph/0408426 [astro-ph].
198. M. Pospelov, *Phys. Rev. Lett.* **98**, 231301 (2007), arXiv:hep-ph/0605215.
199. S. Lola, P. Osland and A. Raklev, *Phys.Lett.* **B656**, 83 (2007), arXiv:0707.2510 [hep-ph].
200. X. Ji, R. N. Mohapatra, S. Nussinov and Y. Zhang, *Phys.Rev.* **D78**, 075032 (2008), arXiv:0808.1904 [hep-ph].
201. W. Buchmuller, A. Ibarra, T. Shindou, F. Takayama and D. Tran, *JCAP* **0909**, 021 (2009), arXiv:0906.1187 [hep-ph].
202. N.-E. Bomark, S. Lola, P. Osland and A. Raklev, *Phys.Lett.* **B686**, 152 (2010), arXiv:0911.3376 [hep-ph].
203. K.-Y. Choi, D. Restrepo, C. E. Yaguna and O. Zapata, *JCAP* **1010**, 033 (2010), arXiv:1007.1728 [hep-ph].
204. B. Holdom, *Phys.Lett.* **B166**, 196 (1986).
205. R. Foot and X.-G. He, *Phys.Lett.* **B267**, 509 (1991).
206. K. R. Dienes, C. F. Kolda and J. March-Russell, *Nucl.Phys.* **B492**, 104 (1997), arXiv:hep-ph/9610479 [hep-ph].

207. A. Ibarra, A. Ringwald and C. Weniger, *JCAP* **0901**, 003 (2009), `arXiv:0809.3196 [hep-ph]`.
208. S. Abel, M. Goodsell, J. Jaeckel, V. Khoze and A. Ringwald, *JHEP* **0807**, 124 (2008), `arXiv:0803.1449 [hep-ph]`.
209. T. Hambye, *JHEP* **0901**, 028 (2009), `arXiv:0811.0172 [hep-ph]`.
210. J. McDonald, *JCAP* **0701**, 001 (2007), `arXiv:hep-ph/0609126 [hep-ph]`.
211. T. Asaka, K. Ishiwata and T. Moroi, *Phys.Rev.* **D75**, 065001 (2007), `arXiv:hep-ph/0612211 [hep-ph]`.
212. C.-R. Chen, F. Takahashi and T. Yanagida, *Phys.Lett.* **B673**, 255 (2009), `arXiv:0811.0477 [hep-ph]`.
213. E. A. Baltz and P. Gondolo, *Phys.Rev.* **D57**, 7601 (1998), `arXiv:hep-ph/9704411 [hep-ph]`.
214. S. Shirai, F. Takahashi and T. T. Yanagida, *Phys. Lett.* **B680**, 485 (2009), `arXiv:0905.0388 [hep-ph]`.
215. D. Aristizabal Sierra, D. Restrepo and O. Zapata, *Phys.Rev.* **D80**, 055010 (2009), `arXiv:0907.0682 [hep-ph]`.
216. K. Hamaguchi, E. Nakamura, S. Shirai and T. Yanagida, *Phys.Lett.* **B674**, 299 (2009), `arXiv:0811.0737 [hep-ph]`.
217. E. Nardi, F. Sannino and A. Strumia, *JCAP* **0901**, 043 (2009), `arXiv:0811.4153 [hep-ph]`.
218. G. 't Hooft, *Phys.Rev.Lett.* **37**, 8 (1976).
219. A. Ibarra and D. Tran, *JCAP* **0807**, 002 (2008), `arXiv:0804.4596 [astro-ph]`.
220. J. Hisano, S. Matsumoto, O. Saito and M. Senami, *Phys.Rev.* **D73**, 055004 (2006), `arXiv:hep-ph/0511118 [hep-ph]`.
221. T. Delahaye, R. Lineros, F. Donato, N. Fornengo and P. Salati, *Phys.Rev.* **D77**, 063527 (2008), `arXiv:0712.2312 [astro-ph]`.